

**MECHANICAL BEHAVIOR OF HYBRID FIBER
REINFORCED CONCRETE UNDER DIRECT
TENSION**

**A Thesis Submitted to
the Graduate School of Engineering and Sciences of
İzmir Institute of Technology
in Partial Fulfillment of the Requirements for the Degree of**

**MASTER OF SCIENCE
in Civil Engineering**

**by
Fatma Şirin ÇETİN**

**June 2020
İZMİR**

ACKNOWLEDGMENTS

I would like to express my sincere gratitude and thanks for my research supervisor Assist. Prof. Dr. Selçuk SAATCI, Department of Civil Engineering, Izmir Institute of Technology. I am also thankful for his scientific advice and continuous support throughout my research.

I would like to thank to my co-supervisor Assoc. Prof. Dr. Tahir Kemal ERDEM, Department of Civil Engineering, Izmir Institute of Technology for his contributions.

I would like to thank to Structural Mechanics Laboratory Technician Cemal Kılıç from Department of Civil Engineering, Izmir Institute of Technology for his supports in experimental parts of this study.

I would like to thank to thesis committee Assoc. Prof. Dr. Engin AKTAŞ and Prof. Dr. Mustafa ŞAHMARAN for their scientific views.

I would like to thank to İzmir Institute of Technology Integrated Research Center and Center for Materials Research, for sharing their experience and guidance.

Finally, I would like to express my deepest thanks to my family for their all of the support throughout my education.

ABSTRACT

MECHANICAL BEHAVIOR OF HYBRID FIBER REINFORCED CONCRETE UNDER DIRECT TENSION

Using different fiber types together, called hybrid fiber reinforced concrete, may cause a mutual synergic response between fiber matrixes. Due to these synergic effects of different fiber combinations, the mechanical behavior of concrete may perform differently than single fiber reinforced concrete.

In this study, the effects of fiber hybridization in the direct tension behavior of concrete mixtures obtained by using three different types of steel fiber and polyvinyl alcohol (PVA) fiber were investigated. In this scope, total of 50 dog bone shaped, notched specimens were cast for 10 different mixtures and tested under direct tension. Average tensile stress-crack width responses of concrete specimens were investigated. It was found that the addition of PVA fiber to 35 mm long single hook end and 60 mm long double hook end steel fiber mixtures with a volume ratio of 0.75% did not considerably change the tensile behavior post cracking. As a result of adding PVA fibers to 60 mm single hook steel fiber mixtures with a volume ratio of 1.25%, cracking stresses were decreased and post cracking behavior was adversely affected. Addition of PVA fibers to 60 mm single hook steel fiber mixture with 0.75% volumetric ratio was found to increase post cracking stress levels.

ÖZET

HİBRİT LİF TAKVİYELİ BETONUN DOĞRUDAN ÇEKME ALTINDA MEKANİK DAVRANIŞI

Hibrit lif takviyeli beton olarak adlandırılan farklı lif türlerinin bir arada kullanılması ile lif matriksleri arasında karşılıklı bir sinerjik tepkiye neden olabilir. Farklı lif kombinasyonlarının bu sinerjik etkileri nedeni ile betonun mekanik davranışı tek lif takviyeli betona göre daha farklı performans gösterebilir.

Bu çalışmada, üç farklı çelik lif tipi ve polivinil alkol (PVA) lif kullanılarak elde edilen beton karışımları ile lif hibritleştirilen betonun doğrudan çekme davranışındaki etkileri araştırılmıştır. Bu kapsamda toplam 50 adet ‘dog bone’ şeklinde çentikli numune 10 farklı karışım için dökülmüş ve doğrudan çekme gerilmesi altında test edilmiştir. Beton numunelerinin ortalama çekme gerilme-çatlak genişliği davranışları incelenmiştir. PVA lifinin hacim oranı % 0.75 olan 35 mm uzunluğunda kısa tek kanca uçlu ve 60 mm uzunluğunda çift kanca uçlu çelik lifli karışımlara eklenmesi sonucu çatlama sonrası gerilme davranışını önemli ölçüde değiştirmedeği bulunmuştur. PVA liflerin hacim oranı % 1.25 olan 60 mm tek kanca uçlu çelik lifli karışımlara eklenmesi sonucunda çatlama gerilmesini azaldığı ve çatlama sonrası davranışı olumsuz etkilediği elde edilmiştir. % 0.75 hacimsel orana sahip 60 mm tekli kanca çelik fiber karışımına PVA liflerinin eklenmesinin, çatlama sonrası gerilme seviyesini arttırdığı bulunmuştur.

TABLE OF CONTENTS

LIST OF FIGURES	vii
LIST OF TABLES.....	xi
CHAPTER 1. INTRODUCTION.....	1
1.1. General Information.....	1
1.2. Objective and Research Significance	6
1.3. Content.....	6
CHAPTER 2. LITERATURE REVIEW	7
CHAPTER 3. EXPERIMENTAL PROGRAM.....	24
3.1. Materials	24
3.2. Mix Design	26
3.3. Tensile Testing of Concrete.....	27
3.4. Preliminary Tests	30
3.5. Direct Tension Tests	40
3.5.1. Test Specimen Geometry	40
3.5.2. Preparation of Wooden Molds	41
3.5.3. Mixing Procedure, Casting and Curing.....	42
3.5.4. Direct Tension Test Setup.....	43
3.5.5. Compressive Strength Test	48
CHAPTER 4. RESULTS AND DISCUSSIONS	50
4.1. Compressive Strength Test Results	50
4.2.. Direct Tension Test Results.....	51
4.3. Discussion of Direct Tension Test Results	68
4.3.1. SF45/35_3D_075 and SF45/35_3D_075+PVA Mixtures	71
4.3.2. SF65/60_3D_075 and SF65/60_3D_075+PVA Mixtures	71
4.3.3. SF65/60_5D_075 and SF65/60_5D_075+PVA Mixtures	72
4.3.4. SF65/60_3D_125 and SF65/60_3D_125+PVA Mixtures	73

CHAPTER 5. CONCLUSIONS	75
REFERENCES	77

LIST OF FIGURES

<u>Figure</u>	<u>Page</u>
Figure 1.1. Types of fibers.....	1
Figure 1.2. Schematic view of fibers bridging cracks	2
Figure 1.3. Load and deflection curve for unreinforced concrete and fiber reinforced concrete	2
Figure 1.4. Different steel fiber types	3
Figure 1.5. Influence of the volume fraction of fibers on the compressive stress- strain curve	4
Figure 1.6. Important characteristics of the load-deflection curve of a fiber reinforced concrete member under flexure	4
Figure 2.1. HyFRC compressive strength test results.....	10
Figure 2.2. Flexural strength of HyFRC	11
Figure 2.3. Load-deflection curves for HyFRC	11
Figure 2.4. Geometrical dimensions and test setup	12
Figure 2.5. Tensile stress-strain curve	13
Figure 2.6. Specimen dimension.....	13
Figure 2.7. Embedded screw with claws	14
Figure 2.8. Stress-strain curve	15
Figure 2.9. Effect of increasing PF ratio.....	15
Figure 2.10. Influence of SF ratio.....	16
Figure 2.11. Test specimen geometry and details.....	17
Figure 2.12. Stress-strain curve	18
Figure 2.13. Experimental setups for compressive test	19
Figure 2.14. Experimental setups for four-point tests	19
Figure 2.15. Compression post-peak behavior: average axial stress vs displacement for HySP-FRCs.	20
Figure 2.16. Average F-CMOD _m curves for HySP-FRCs.....	20
Figure 2.17. Fracture test results: average curve of three specimens of each concrete type.....	21

<u>Figure</u>	<u>Page</u>
Figure 2.18. Uniaxial test result: average curves of two specimens of each concrete type.....	22
Figure 3.1. Splitting test.....	28
Figure 3.2. Three-point bending test.....	28
Figure 3.3. Three-point bending test.....	28
Figure 3.4. Four-point bending test	29
Figure 3.5. Axial tension test - notched cylinder	29
Figure 3.6. Specimen shape and dimensions for adopted size range.....	31
Figure 3.7. Preliminary test specimen geometry	31
Figure 3.8. Test specimens	35
Figure 3.9. Test setup preliminary studies	37
Figure 3.10. Test results for T1	37
Figure 3.11. Test results for T2.....	38
Figure 3.12. Test results for T3.....	38
Figure 3.13. Test results for T4.....	39
Figure 3.14. Test results for T5.....	39
Figure 3.15. Force-displacement curve for T6	40
Figure 3.16. Specimen cross section (dimensions are mm).....	41
Figure 3.17. Wood mold	42
Figure 3.18. Rotating drum mixer	42
Figure 3.19. Test setup drawing.....	44
Figure 3.20. Test specimen	45
Figure 3.21. Test setup.....	46
Figure 3.22. Digital movement gauge	46
Figure 3.23. Test specimen	47
Figure 3.24. Measuring manually	47
Figure 3.25. Avg crack width- stroke graph	48
Figure 3.26. Cylinder specimens	49
Figure 3.27. Digital compressive test machine.....	49
Figure 4.1. Compressive strength test results	51
Figure 4.2. SF45/35_3D_075-1 specimen after cracking	54

<u>Figure</u>	<u>Page</u>
Figure 4.3. SF45/35_3D_075-2 specimen after cracking	54
Figure 4.4. SF45/35_3D_075-3 specimen after	55
Figure 4.5. Stress-crack width curve for SF45/35_3D_075 (SFRC).....	55
Figure 4.6. SF45/35_3D_075+PVA-1 specimen after cracking.....	56
Figure 4.7. SF45/35_3D_075+PVA-2 specimen after cracking.....	56
Figure 4.8. SF45/35_3D_075+PVA-3 specimen after cracking.....	56
Figure 4.9. Stress-crack width for SF45/35_3D_075+PVA(HyFRC).....	57
Figure 4.10. SF65/60_3D_075-1 specimen after cracking.....	57
Figure 4.11. SF65/60_3D_075-2 specimen after cracking	58
Figure 4.12. Stress–crack width curve for SF65/60_3D_075 (SFRC)	58
Figure 4.13. SF65/60_3D_075+PVA-2 specimen after cracking.....	59
Figure 4.14. SF65/60_3D_075+PVA-3 specimen after cracking.....	59
Figure 4.15. Stress–crack width curve for SF65/60_3D_075+PVA (HyFRC)	60
Figure 4.16. SF65/60_5D_075-1 specimen after cracking	60
Figure 4.17. SF65/60_5D_075-2 specimen after cracking	61
Figure 4.18. Stress-crack width curve for SF65/60_5D_075 (SFRC).....	61
Figure 4.19. SF65/60_5D_075+PVA-2 specimen after cracking.....	62
Figure 4.20. SF65/60_5D_075+PVA-3 after cracking.....	62
Figure 4.21. Stress-crack width curve for SF65/60_5D_075+PVA (HyFRC).....	63
Figure 4.22. SF65/60_3D_125-1 specimen after cracking	63
Figure 4.23. SF65/60_3D_125-2 specimen after cracking	64
Figure 4.24. Stress-crack width curve for SF65/60_3D_125 (SFRC).....	64
Figure 4.25. SF65/60_3D_125+PVA-1 specimen after cracking.....	65
Figure 4.26. SF65/60_3D_125+PVA-2 specimen after cracking.....	65
Figure 4.27. Stress-crack width curve for SF65/60_3D_125+PVA (HyFRC).....	66
Figure 4.28. PVA group specimen after cracking	66
Figure 4.29. PVA group specimen after cracking	67
Figure 4.30. PVA group specimen after cracking	67
Figure 4.31. Normal concrete group specimen after cracking.....	67
Figure 4.32. Average tensile cracking strength	68
Figure 4.33. Average energy consumed of each mixtures.....	68

<u>Figure</u>	<u>Page</u>
Figure 4.34. Average tensile stress-crack width curves.....	69
Figure 4.35. Average tensile stress-crack width curves.....	70
Figure 4.36. Average stress-crack width curves	71
Figure 4.37. Average stress-crack width curves	72
Figure 4.38. Average stress-crack width curves	73
Figure 4.39. Average stress-crack width curves	74

LIST OF TABLES

<u>Table</u>	<u>Page</u>
Table 2.1. Fiber contents of specimens.....	7
Table 2.2. Fiber properties	8
Table 2.3. Compressive strength test results.....	8
Table 2.4. Flexural tensile strength test results.....	9
Table 2.5. HyFRC mixture proportions	10
Table 2.6 Mix proportions with different fiber ratios.....	12
Table 2.7. Mix design proportions.....	21
Table 3.1. Specific gravity and absorption capacity of fine and coarse aggregates	24
Table 3.2. Properties of the superplasticizer	25
Table 3.3. Mechanical properties of PVA	25
Table 3.4. Mechanical properties of steel fibers	26
Table 3.5. HyFRC mixture proportions	27
Table 3.6. Preliminary test specimens	32
Table 4.1. Compressive strength test results.....	50
Table 4.2 Direct tension test results.....	52-53

CHAPTER 1

INTRODUCTION

1.1. General Information

Concrete is one of the common construction materials which consists of coarse aggregate, cementing material, water and fine aggregate. The main advantage of concrete is its high compressive strength. However, it has a weak tensile strength and it is brittle under tensile loading.

Fibers are one of the reinforcing materials used to overcome the weak tensile strength of concrete. Fibers are used to enhance the mechanical properties of concrete and its structural integrity. Fibers are produced in various materials and in different forms, including glass, steel, carbon, polymer fibers (Figure 1.1.).



Figure 1.1. Types of fibers

Fiber reinforced concrete is described as concrete including hydraulic cements, aggregates and discontinuous discrete fibers. The performance of fibers in concrete depends on matrix properties together with fiber type, fiber volume in concrete mixture, fiber geometry, fiber orientation, and fiber distribution (ACI Committee 544, 1999).

Concrete has low tensile strength and has a brittle tensile behavior due to sudden formation and propagation of micro cracks. Addition of fibers to concrete enhance the mechanical properties of the concrete by bridging across the cracks progressing in the

matrix, thus preventing the spread of micro-cracks and postponing the initial stage of tension cracks (Alami et al, 2018). Furthermore, bridging the cracks cause the transfer of tensile stresses to the concrete matrix and result in multiple cracking in concrete. This behavior continues until the fibers break or deboned from concrete, increasing the fracture toughness (Figure 1.2.). A typical concrete member without fibers exhibit a sudden loss of capacity after cracking under tension. However, a fiber reinforced concrete member continues to carry load after cracking due to this mentioned mechanism (Figure 1.3.).

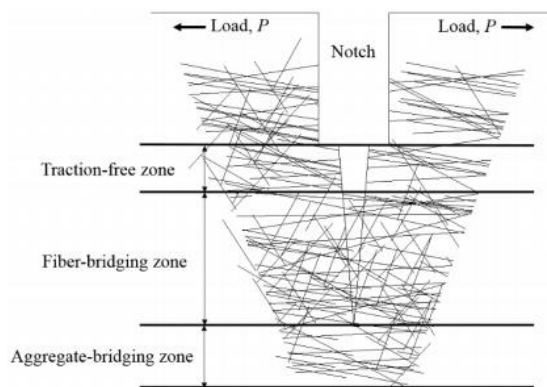


Figure 1.2. Schematic view of fibers bridging cracks
(Source: Kim and Bordelon, 2017)

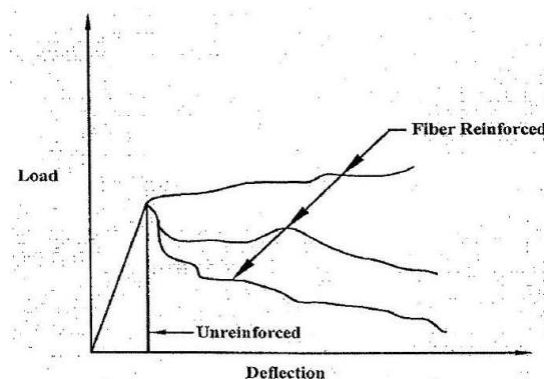


Figure 1.3. Load and deflection curve for unreinforced concrete and fiber reinforced concrete (Source: ACI Committee 544, 2002)

Steel fibers are the most commonly used fiber type in fiber reinforced concrete members. There are several types of steel fibers as seen on Figure 1.4. The mechanical properties of steel fiber reinforced concrete are dependent on the type of fiber, the amount of fiber, aspect ratio and the size of aggregates. The mechanical properties of the member are influenced by fiber performance with respect to direct tension, bending, impact and

shear. The stress caused by these loads is shared by fiber and matrix in tension until this total stress are transferred by the fibers or matrix cracks (ACI Committee 544, 1999).

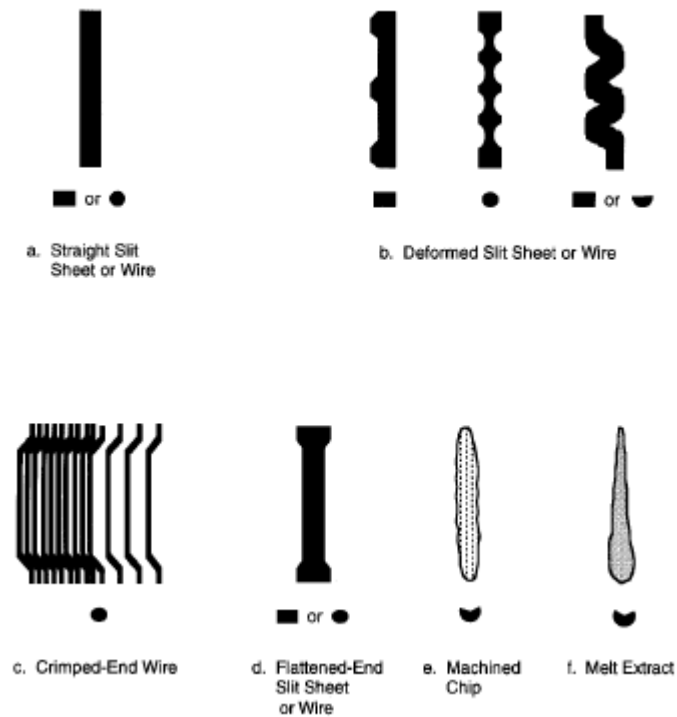


Figure 1.4. Different steel fiber types
(Source: ACI Committee 544, 2002)

Steel fibers do not considerably affect the compressive strength of concrete. Figure 1.5. shows a typical compressive behavior of concrete under compression with increasing fiber ratio. As seen in the figure, addition of fibers enhance strain at the ultimate stress and post peak stress drop becomes more gradual compared to concrete without fibers. In other words, steel fibers supply post cracking ductility and increase toughness, which is the ability of energy absorption during deformation. This descending part of stress-strain curve depends on fiber type and shape, fiber volumetric ratio, fiber aspect ratio and mix design of concrete matrix (ACI Committee 544, 1999).

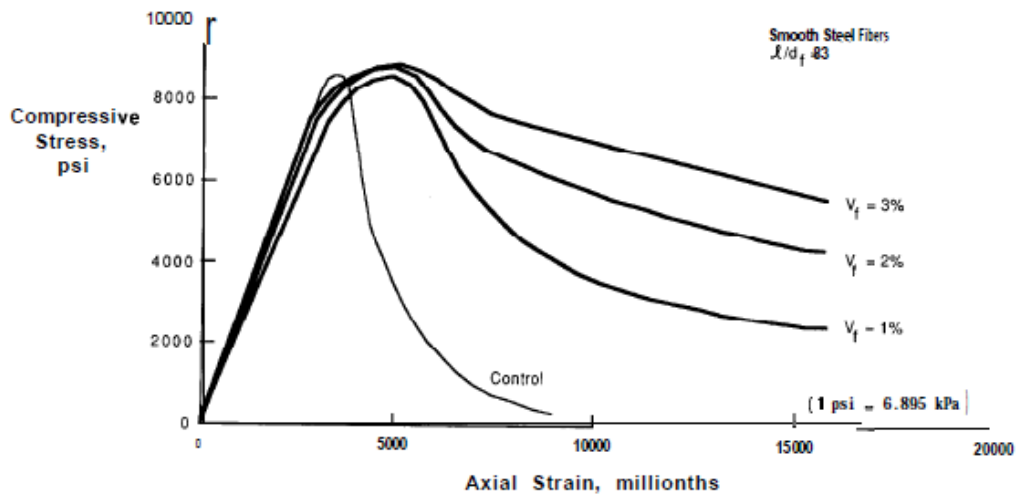


Figure 1.5. Influence of the volume fraction of fibers on the compressive stress-strain curve (Source: ACI Committee 544, 1999)

Steel fibers perform better performance in improving flexural strength of concrete. For the load-deflection curve of a typical member under flexure, first crack account for the load deformation curve separated from the linearity, as can be seen in Figure 1.6. at point A. The point C in Figure 1.6. marks the ultimate flexural strength or modulus of rupture. This point is related to fiber amount and aspect ratio (ACI Committee 544, 1999).

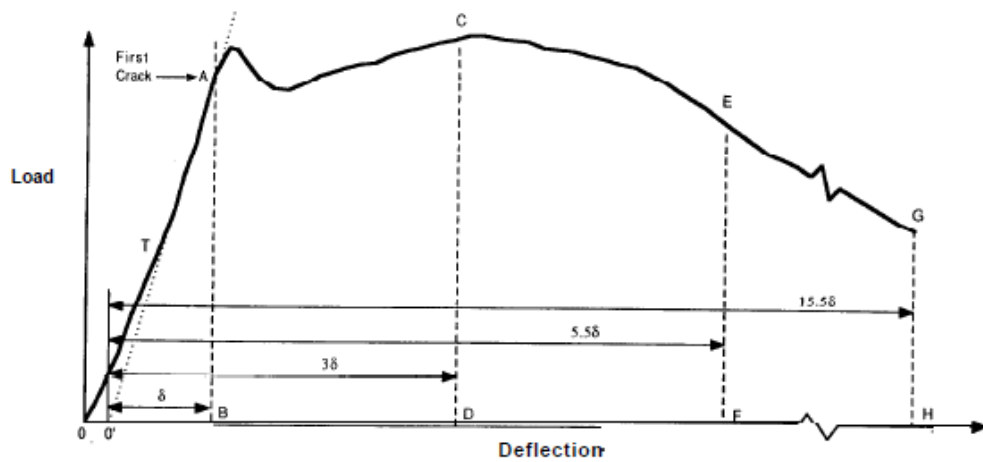


Figure 1.6. Important characteristics of the load-deflection curve of a fiber reinforced concrete member under flexure (Source: ACI Committee 544, 1999)

Aside from steel fibers, synthetic fibers are also used as a construction material for the reinforcement of cementitious materials. Synthetic fibers can be made of several types of materials, including aramid, acrylic, nylon, carbon, polyester, polyethylene,

polypropylene and polyvinyl alcohol (ACI Committee 544, 2002). They are produced by different properties in terms of shape and size.

Polypropylene and polyvinyl alcohol fibers are most commonly used synthetic fibers in concrete. Polypropylene fiber has advantages with its high melting point (165°C), high alkali resistance and low-cost raw material. However, its sensitivity to oxygen and sunlight, lower modulus of elasticity and weak bond with matrix can be listed as its disadvantages. Polypropylene fibers can improve tensile behavior post cracking. However, this increase is not significant (Bentur and Mindess, 2006).

Polyvinyl alcohol (PVA) fibers are produced by dry or wet spinning. By adding boron, intermolecular bonds are formed, and thus high strength and hardness are obtained. PVA fibers are surface treated in order to make efficient dispersion and to increase compatibility with matrix have OH polymer groups are involved in this surface treatment and when this polymer is combined with its natural affinity to water, they form an efficient dispersion and strong bond in the stiffened composite (Bentur and Mindess, 2006).

Hybrid reinforced concrete includes two or more fiber types. Fibers can be added to concrete mixture with varying materials, length and aspect ratio. Applications of hybrid reinforced concrete can be discussed in terms of fiber type, proportion and mix design. Adding short discontinuous fibers contribute to significant development of mechanical property of concrete. In hybrid fiber composites, there is a mutual effect between the fibers and the resultant hybrid performance exceeds the total of singular fiber performances. This phenomenon is called “Synergy”.

The presence of stronger and stiffer fibers in hybrid composites improves the initial tension cracking and peak strength, and the presence of flexible and ductile fibers increases toughness and strain levels at the post-cracking region. Shorter fiber types supply a reinforcement that bridges micro-cracks and can control crack growth. Longer fibers control propagation of macro cracks and may greatly increase the toughness index. Fibers with different strengths have a positive total effect on hybrid reinforcement concrete. The fibers that has high durability enhance property of toughness and strength after age. The fibers that has low durability supply the short-term performance of the composites. (Bentur and Mindess, 2006). These fibers can prevent cracking in concrete during erection and transportation in precast concrete members.

1.2. Objective and Research Significance

Hybrid reinforced concrete (HyFRC) is relatively a new composite and significant research efforts are still being spent on the investigation of the mechanical behavior of this material. Due to the wide variety of the possibilities in mixing different types of fibers, these efforts are rather dispersed, each focusing on particular fiber types and mix. The objective of this research is to investigate the mechanics of HyFRC in more general terms, focusing on effects of different fiber types, fiber lengths and fiber ratios. Direct tension and compression capacities of various HyFRC samples are investigated and observed behavior is compared to single fiber composites. The results obtained from this study are expected to contribute to the characterization of the mechanical properties of HyFRC.

1.3. Content

This research includes an experimental study conducted at İzmir Institute of Technology.

In the following chapter, the literature on hybrid fiber concrete was reviewed. Direct tensile tests, their implementation and concrete specimen geometries were examined from the literature. Results of direct tensile, compression and bending tests were examined and current knowledge on the effect of different fibers on post-cracking strength and toughness properties were reviewed.

In the third chapter, experimental program conducted in this study was presented. Material details, mixture design, previous experimental studies and direct tensile test equipment were explained.

In the fourth chapter, results and discussions of the tests performed during this study were discussed. The analysis of the results was presented in this section.

In the fifth chapter, conclusion was presented.

CHAPTER 2

LITERATURE REVIEW

In this chapter, significant studies on hybrid reinforced concrete are presented with a focus on the direct tension testing.

In a study by Yurtseven (2004) mechanical properties (Compressive strength, flexural tensile strength and toughness, and impact resistance) of hybrid fiber concrete were investigated. Four different types of fibers were used with total 1.5% volumetric ratio (Table 2.1.). Dramix RC 80/60 and Dramix ZP 305 were used as macro steel fibers, whereas OL 6/16 were used as micro steel fibers. Duomix 20 was used as polypropylene fiber (Table 2.2.).

Table 2.1. Fiber contents of specimens
(Source: Yurtseven, 2004)

Mix No	Designation	Volume Percentage of Fiber Contents (%)			
		R	Z	L	D
1	Control	0.0	0.0	0.0	0.0
2	R1.5	1.5	0.0	0.0	0.0
3	R1.0L0.5	1.0	0.0	0.5	0.0
4	R1.0L0.3D0.2	1.0	0.0	0.3	0.2
5	R1.0D0.5	1.0	0.0	0.0	0.5
6	Z1.5	0.0	1.5	0.0	0.0
7	Z1.0L0.5	0.0	1.0	0.5	0.0
8	Z1.0L0.3D0.2	0.0	1.0	0.3	0.2
9	Z1.0D0.5	0.0	1.0	0.0	0.5

Table 2.2. Fiber properties
(Source: Yurtseven, 2004)

Fiber Name	Designation	Density (kg/m ³)	Length (mm)	Diameter (mm)	Min f_t * (MPa)	Geometry
Dramix RC 80/60	R	7850	60	0.75	1050	Hooked
Dramix ZP 305	Z	7850	30	0.55	1100	Hooked
OL 6/16	L	7170	6	0.16	2000	Straight
Duomix 20	D	910	20	0.016	400	Fibrillated

* Minimum tensile strength of the wire

According to the study, compressive strength increased with fiber inclusion for all types. However, increasing fiber ratio was not effective considerably in the compressive strength. (Table 2.3).

Table 2.3. Compressive strength test results
(Source: Yurtseven, 2004)

Mix Designation	f_{comp} 28 Days (MPa)			Average	
	1	2	3	(MPa)	St. Dev.
Control	36.80	37.50	37.32	37.21	0.36
R1.5	40.46	40.46	38.80	39.91	0.96
R1.0L0.5	42.73	43.08	42.73	42.85	0.20
R1.0L0.3D0.2	42.73	41.42	42.90	42.35	0.81
R1.0D0.5	36.28	37.67	38.37	37.44	1.06
Z1.5	40.64	40.98	42.03	41.22	0.72
Z1.0L0.5	45.52	45.26	45.34	45.37	0.13
Z1.0L0.3D0.2	41.94	41.16	41.42	41.51	0.40
Z1.0D0.5	37.50	37.84	37.50	37.61	0.20

Tensile flexural results in this study showed that there was significant strength gain with fiber in concrete. R1.0L0.5 composite had highest tensile strength and Z1.0L0.3D0.2 had lowest tensile strength. It can be said that the macro fiber RC 80/60 was more efficient than macro steel fiber ZP 305 in improving tensile strength. It is observed that the composites with micro OL 6/16 steel fiber and macro steel fiber showed better flexural tensile strength than only macro steel fiber composites. On the other hand, there was no synergy response between OL 6/16 and polypropylene fiber Duomix 20. These fiber combinations showed low tensile strength performance (Table 2.4.).

Table 2.4. Flexural tensile strength test results
(Source: Yurtseven, 2004)

Mix Designation	f_{flex} (MPa)		Average	
	1	2	(MPa)	St. Dev.
Control	5.0	4.6	4.8	0.28
R1.5	8.6	9.0	8.8	0.28
R1.0L0.5	10.4	11.6	11.0	0.85
R1.0L0.3D0.2	7.8	7.0	7.4	0.57
R1.0D0.5	7.4	8.2	7.8	0.57
Z1.5	7.2	6.0	6.6	0.85
Z1.0L0.5	7.2	8.0	7.6	0.57
Z1.0L0.3D0.2	6.0	6.8	6.4	0.57
Z1.0D0.5	6.6	7.0	6.8	0.28

In a study by Alami et al. (2018) Engineered Cementitious Composites (ECC) and Hybrid Fiber Reinforced Concrete (HyFRC) was investigated for deflection hardening under four-point bending. ECC was produced alone with synthetic PVA fibers and fine aggregate, and HyFRC was generated with fine aggregate, coarse aggregate and steel and synthetic PVA fibers.

In this study, HyFRC mixtures' binder (fly ash and portland cement) content was 600 kg/m^3 and the coarse aggregate D_{max} was selected as 8 mm or 16 mm. Mixing ratios of HyFRC is presented in Table 2.5. Three types of fibers, Dramix® 40/30 3D, Dramix® 65/60 3D and Dramix® 65/60 5D were used in this study and these were named ST1, ST2, and ST3 respectively. Naming of the mixtures were chosen as “steel fiber type, steel fiber ratio_ P-PVA ratio_D-maximum aggregate size in mm”. For instance, ST2,0.75_P0.25_D8 is for 65/60 3D steel fiber 0.75 % ratio by volume, 0.25% by volume PVA fibers, 8 mm maximum aggregate size. Specimens with perlite aggregates were also tried by replacing 20% of the fine aggregate with perlite. For these specimens, last part of the naming convention was changed to “Per20”. River sand and coarse aggregate were named as RS and CA, respectively.

Table 2.5. HyFRC mixture proportions
(Source: Alami et al., 2018)

Mix	PC	FA/PC	Water/Binder	RS	CA	Steel fiber (Vol%)	PVA (Vol%)
1	1	1.2	0.40	2.3	2.5	0.50	0.25
2	1	1.2	0.40	2.3	2.5	0.50	0.50
3	1	1.2	0.40	2.3	2.5	0.75	0.25
4	1	1.2	0.40	2.3	2.5	0.75	0.50
5	1	1.2	0.40	2.3	2.5	1.25	0.25
6	1	1.2	0.40	2.3	2.5	1.25	0.50

In this study, standard cylinder tests were cast according to EN 206-1, and ASTM C 39. Three specimens of each mixture were tested with rate of 0.038 mm/sec by a digital compression machine. According to test results, average compressive strength of HyFRC was found between 34 and 40 MPa and the average compressive strength of normal concrete (without fibers) was 30 MPa. When these results were examined, it was found that there was no significant gain in compressive strength. However, it was found that compressive strength was higher in mixtures with large aggregate diameter. It was mentioned that the aggregate size could have significant effects on compressive strength. However, the change in compressive strength has a negligible effect on the comparison of concrete with different fiber ratios containing the same aggregate sizes (Figure 2.1.).

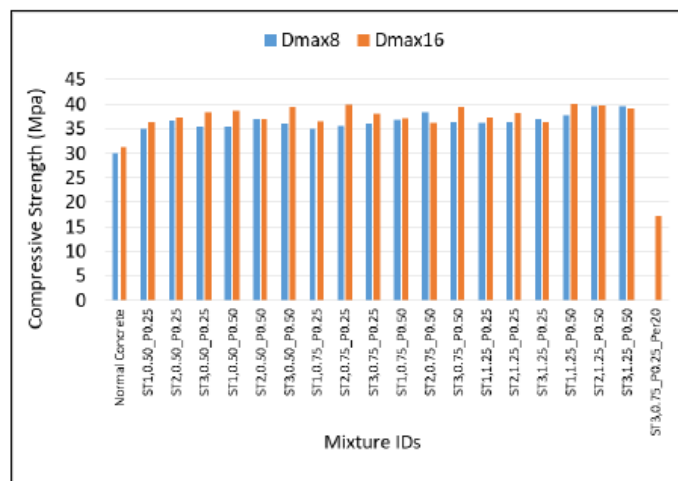


Figure 2.1. HyFRC compressive strength test results
(Source: Alami et al., 2018)

Alami et al. (2018) also performed four-point bending tests and obtained load-deflection curves for HyFRC beam specimens. According to test results, flexural strength and toughness improved with increasing Dmax and but they decreased when the PVA volume in the mixtures increased from 0.25 to 0.5%. Moreover, it was found that the flexural strength and toughness increased as the steel fiber ratio increased. Alami et al. (2018) compared the flexural behavior of 36 different mixes and selected six of them to be the best according to their flexural performance (Figure 2.2. and Figure 2.3.). Note that these mixes were adopted in this thesis work as well.

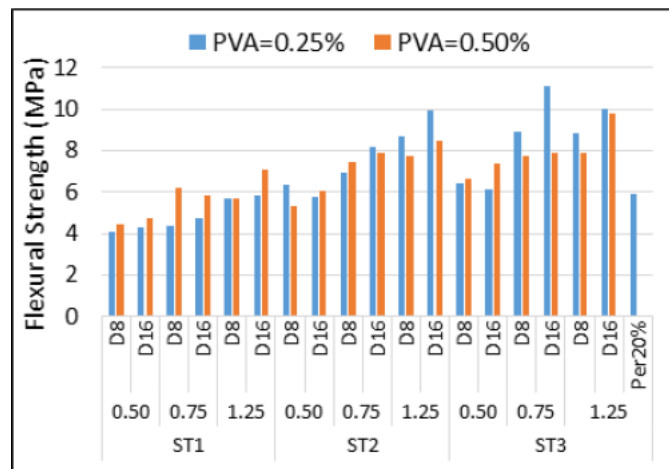


Figure 2.2. Flexural strength of HyFRC (Source: Alami et al., 2018)

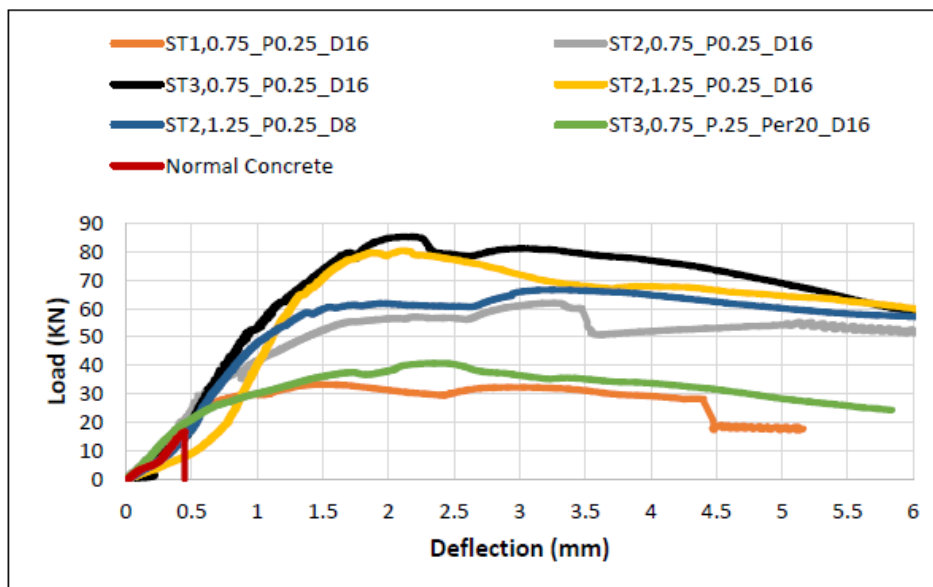


Figure 2.3. Load-deflection curves for HyFRC (Source: Alami et al., 2018)

There are numerous studies in the literature involving direct tension test of fiber reinforced concrete. In a study by Mathew et al. (2015), an analytical and experimental research on High Strength Steel Fiber Reinforced Concrete (HS-SFRC) was conducted. In this study, mechanical properties such as compressive strength, splitting tensile strength and direct tension test were examined to find out how much mechanical properties improve with changing fiber volumetric ratio. The circular-double-end hooked steel fiber was used in this research. Mixture designs of the specimens are shown in Table 2.6. DB-0 represents control group, DB-1 and DB-2 represent steel fiber reinforced concrete with 0.5% and 1% volumetric ratio, respectively.

Table 2.6 Mix proportions with different fiber ratios
(Source: Mathew et al., 2015)

Description	DB - 0	DB - 1	DB - 2
Binder Content (kg/m ³)	435	435	435
Cement (kg/m ³)	348	348	348
Silica Fume (kg/m ³)	43.5	43.5	43.5
Fly Ash (kg/m ³)	43.5	43.5	43.5
Fine Aggregate (kg/m ³)	827	827	827
Coarse aggregate (kg/m ³)	1050	1050	1050
Water (l/m ³)	145	145	145
Super Plasticizer (l/m ³)	4.44	4.44	4.44
Steel Fibre (kg/m ³)	0	39.25	78.50

In this study, direct tension test was carried out with a universal test machine with a computerized displacement control. The loading was applied at a tensile speed of 0.6 mm / min. Dimensions of the specimens in the form of a dog bone and the setup used for direct tension tests are presented in Figure 2.4.

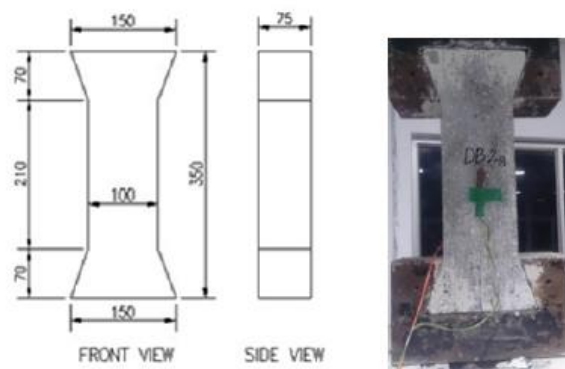


Figure 2.4. Geometrical dimensions and test setup
(Source: Mathew et al., 2015)

As a result of the direct tension tests, they found that the post-cracking behavior of fiber reinforced concrete was better compared to normal concrete specimen, in a sense that they showed much higher toughness and deformation capability (Figure 2.5).

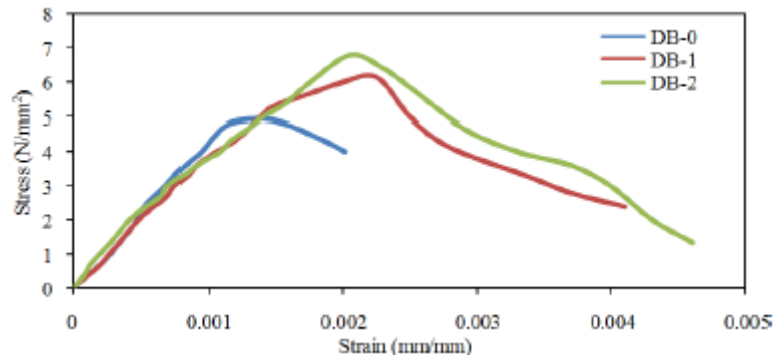


Figure 2.5. Tensile stress-strain curve
(Source: Mathew et al., 2015)

In a study by Xu et al. (2016), mechanical properties of HyFRC were investigated under uniaxial tension tests. This study involved shear corrugated steel fiber (SF) and monofilament polypropylene fibers (PF). SFs were used with 1.1, 1.5, and 1.9% in volume and their aspect ratios (length to diameter) were 30, 60, and 80, respectively. PFs were used in 0.11%, 0.15% and 0.19% in volume with a constant aspect ratio of 396. Dog bone shape specimens were designed with a variable cross section as seen in Figure 2.6.

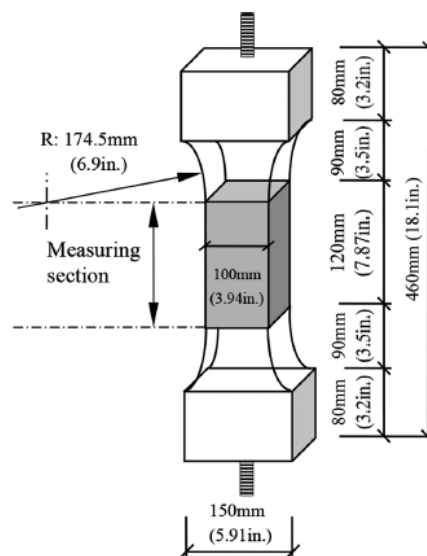


Figure 2.6. Specimen dimension
(Source: Xu et al., 2016)

A threaded screw with a diameter of 20 mm was embedded at each end of specimens at a depth of 150 mm. Threaded screw had a steel wire tab to avoid potential pullout failure due to stress concentration as seen in Figure 2.7.

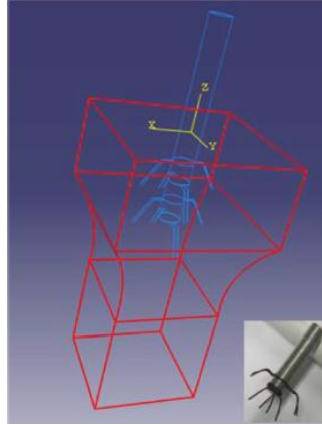


Figure 2.7 Embedded screw with claws
(Source: Xu et al.,2016)

For this study, uniaxial tension tests were performed by using a universal testing machine by controlling displacement at a 0.04 mm/min loading rate. A special experiment test setup was used with loading fixtures and spherical joints. As a result of the study, influence of SF, influence of PF and influence of aspect ratios were examined in terms of tensile strength. In Figure 2.8. and Figure 2.9., stress-strain responses of test specimens are given. In these figures, specimens were named as “SB-SF fiber ratio-P-PF fiber ratio”. PC refers to control specimen with no fibers. In this research, SF contents were 1.1, 1.5, and 1.9% with three aspect ratios of 30, 60, and 80. The PF contents were 0.11%, 0.15% and 0.19% with a same aspect ratio of 396. For example, SB11P11 identifies that steel fiber content is 1.1 % with aspect ratio is 60, PF amount is 0.11%.

As seen in Figure 2.8. stress-strain responses were improved by using hybrid fibers in terms of observed peak strength and deformation capacity. Furthermore, it can be seen that the peak tensile strength and pre-peak stiffness increase slightly as SF is added.

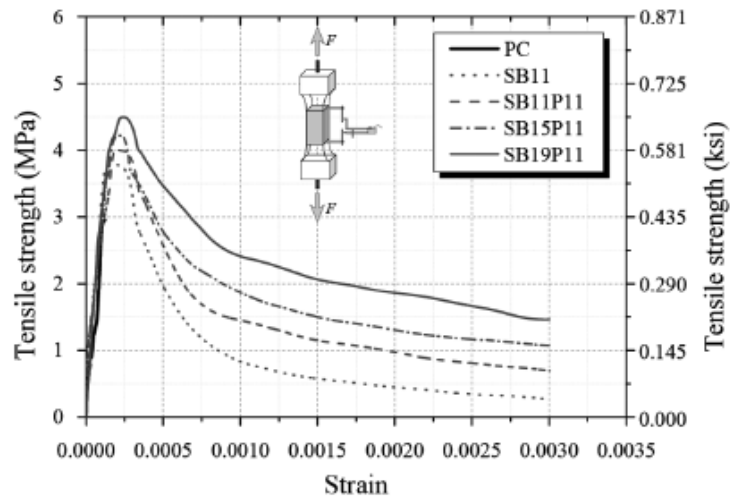


Figure 2.8. Stress-strain curve
(Source: Xu et al ,2016)

Figure 2.9. shows the effect of increasing PF ratio. As can be seen, the area under the curves after peak is clearly increased with increasing ratio of PF.

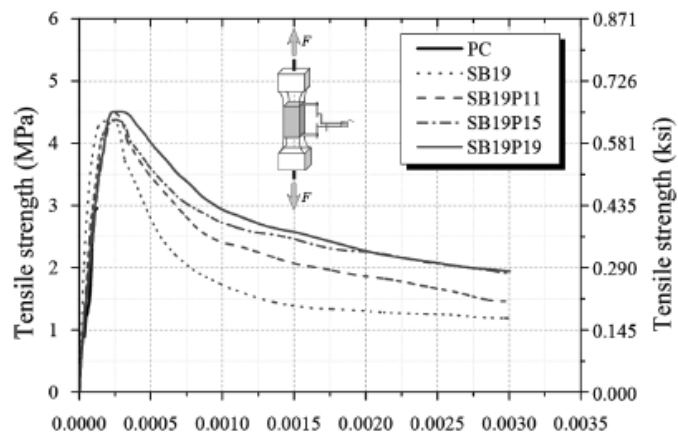


Figure 2.9. Effect of increasing PF ratio
(Source: Xu et al., 2016)

Figure 2.10. presents the influence of SF ratio on the tensile strength for a constant fiber aspect ratio. It is seen from this figure that the tensile strength is directly proportional to the increase of steel fiber ratio.

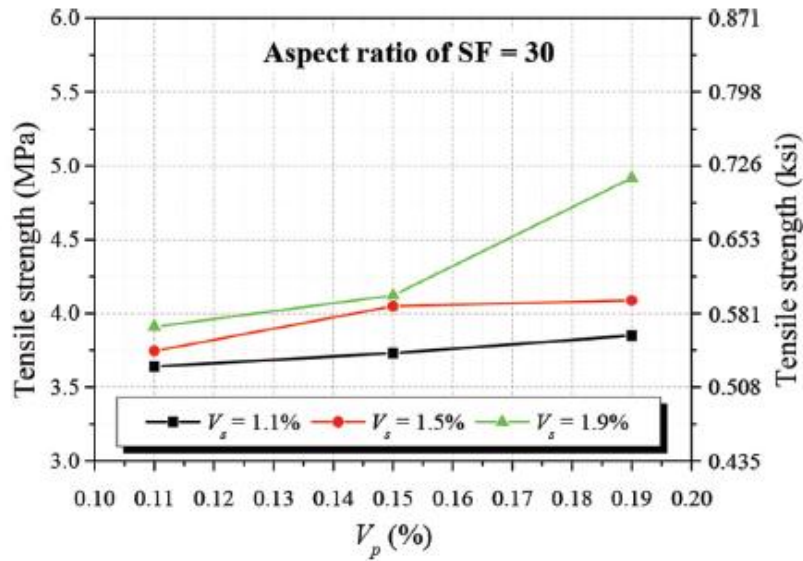


Figure 2.10. Influence of SF ratio
(Source: Xu et al.,2016)

As a result of this study, it was found that the deformation capability, ductility and tensile strength of concrete were considerably increased by using steel-polypropylene hybrid fibers. Tensile strength was increased between 25 to 80 percent with respect to PC. This effect was attributed to the synergy created by hybridization. It was also found that steel fibers played a major role in the hybrid system. However, polypropylene fibers improved the residual strength in post-peak region.

Chasioti and Vecchio (2017) studied the effect of synergy on tensile strength, fracture toughness and displacement capacity in direct tension concrete specimens. Dog-bone shaped specimens were used which were mounted to a 245 kN universal testing machine with threaded rods. Tests were performed with controlled displacement using one LVDT on each side of the sample at a 0.001 mm/s loading rate until a peak load, and then afterwards gradually increased until it reached a maximum of 0.01 mm / s. A novel specimen design was used for direct tension tests. In the specimens, end regions were strengthened and thus regressions were reached to the middle part to cause failure in the prismatic part of the sample where the sample had no shape effects. In addition, end zones were reinforced with a grid of two layers of steel wire mesh. Threaded rods were embedded in specimens from both ends, meeting at the middle. Rods were aligned in the middle with a wooden piece and middle part was wrapped with plastic, so that threaded rods will not come in contact with concrete and entire load will be carried by concrete in this region (Figure 2.11.).

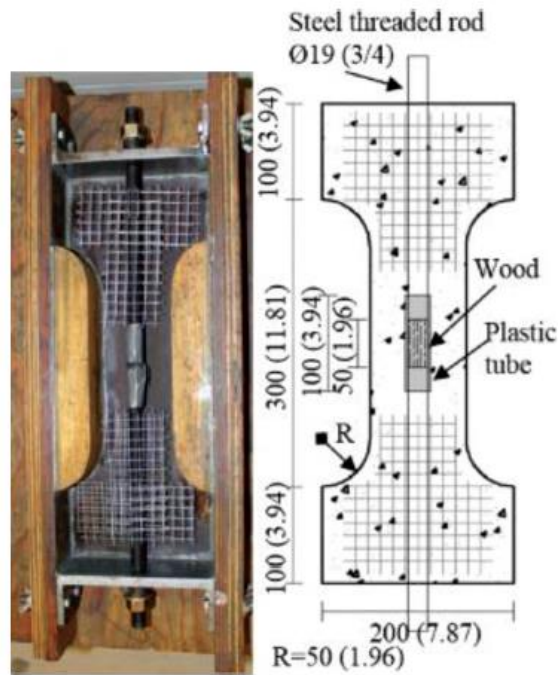


Figure 2.11. Test specimen geometry and details
(Source: Chasioti and Vecchio ,2017)

An experimental study involving normal strength concrete using two types of steel fibers was carried out: 13 mm long high strength flat steel microfibers and 30 mm long hook-end macrofibers. Eight different concrete mixtures were poured. In the specimen names, Hy identifies hybrid fibers, SL identifies single long fiber (macrofiber), SS identifies single short fiber (microfiber) in the mix. Total fiber ratios are equal to 0.75%, 1.0%, 1.5%, and 2.0%.

According to test results it was observed that high total fiber ratios resulted in higher strength after cracking. In direct tension, fracture energy and post-cracking strength were increased with fiber hybridization. The synergy that is between fibers is enhanced at higher whole fiber ratios. However, Hy2.0 mixture had lower strength than Hy 1.5 (Figure 2.12.).

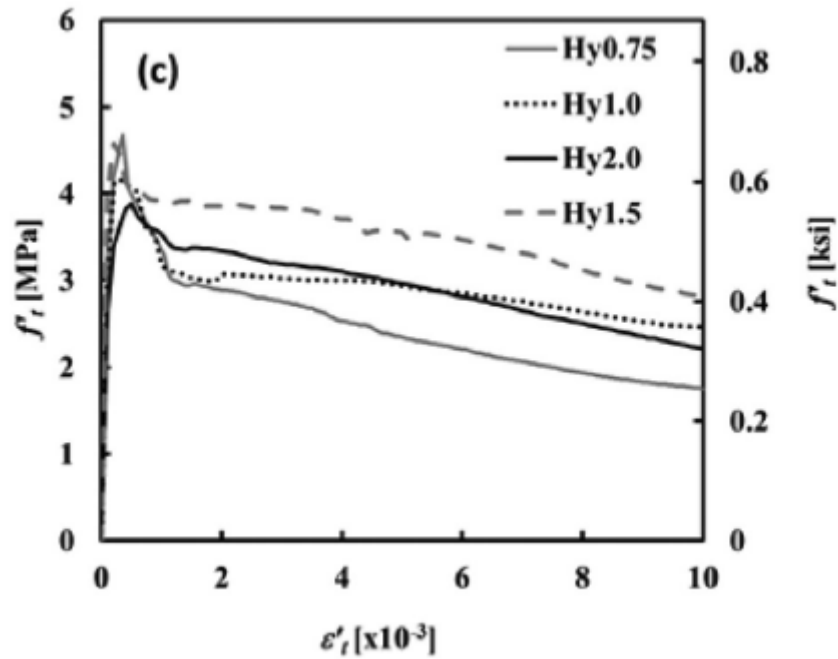


Figure 2.12. Stress-strain curve
(Source: Chasioti and Vecchio, 2017)

In the study of Chasioti and Vecchio (2017), synergistic effects in strength, stiffness and toughness were observed for the tested fiber combinations. It should be noted that synergistic effects could vary for other fiber combinations. However, it was verified that HySFRC as a viable and economical alternative to single fiber reinforced concrete.

Caggiano et al. (2016) performed tests with using polypropylene and steel fibers in concrete mixtures. They tried five mixtures with different polypropylene and steel fiber percentages but identical total volume of fiber. They performed four-point bending tests and compressive strength tests on the specimens. Compressive strength test was performed at 0.005 mm/min rate with displacement control according to EN 12390-4. During tests, for measuring local strains, three strain gauges (horizontal and vertical) were glued at the mid-height of specimens, arranged to be 60 degrees apart from each other (Figure 2.13.). Four-point bending tests were performed at a 0.005 mm/min displacement rate. Crack Mouth Opening Displacement (CMOD), which is the relative displacement between two points of notches at the bottom, were also measured in these tests (Figure 2.14.).

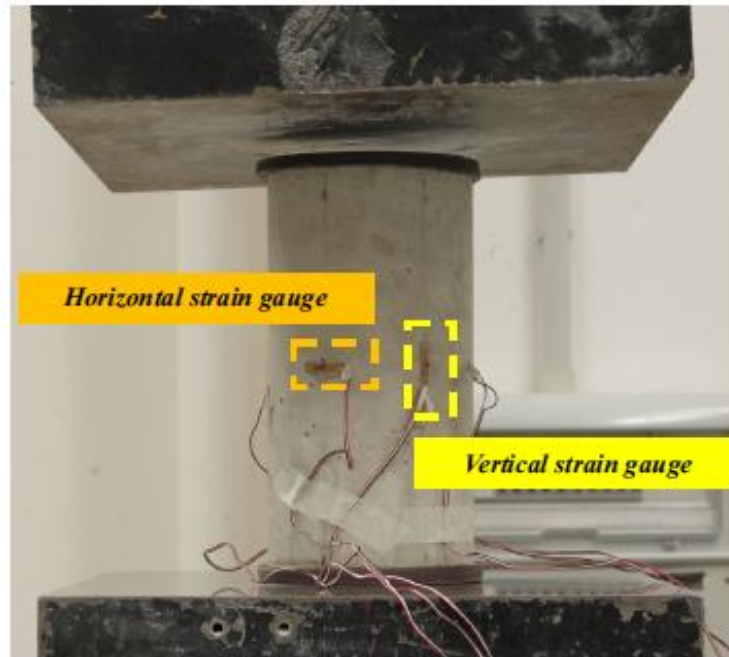


Figure 2.13. Experimental setups for compressive test
(Source: Caggiano et al., 2016)

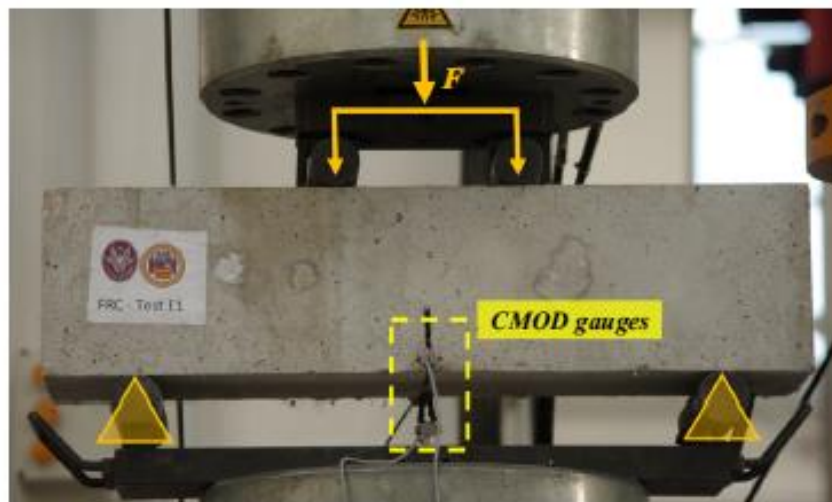


Figure 2.14. Experimental setups for four-point tests
(Source: Caggiano et al., 2016)

The authors found that compressive strength was not significantly affected by the presence of fibers (Figure 2.15.).

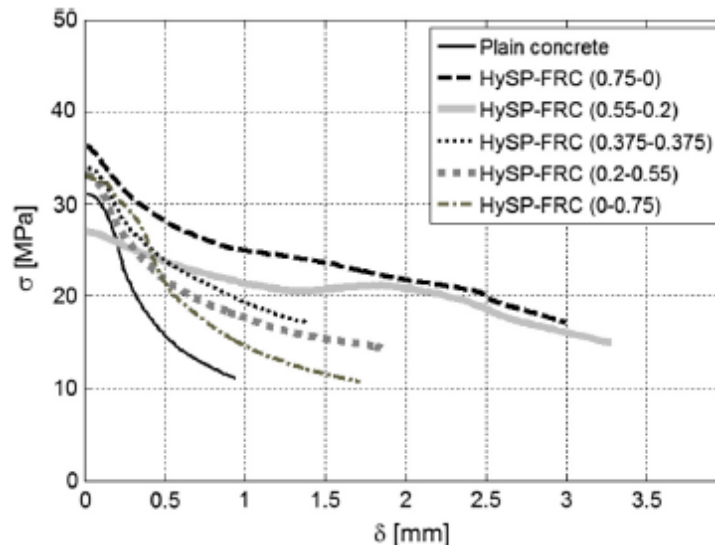


Figure 2.15. Compression post-peak behavior: average axial stress vs displacement for HySP-FRCs. (Source: Caggiano et al., 2016)

According to the four-point bending test results of the study, increasing steel fiber percentages in concrete caused higher post-cracking strength and increase in toughness was observed. However, as seen in Figure 2.16., increasing the percentage of polypropylene fibers lead to decreasing strength and toughness of HyFRC mixture.

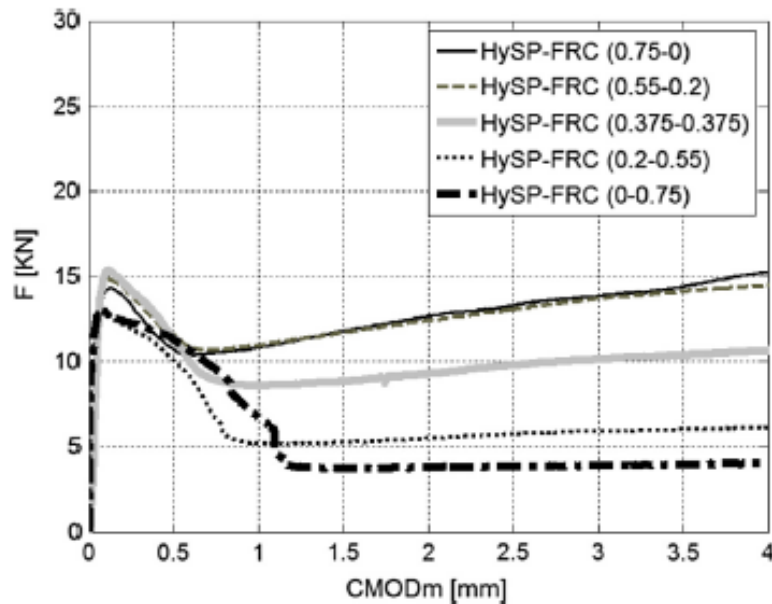


Figure 2.16. Average F-CMODm curves for HySP-FRCs. (Source: Caggiano et al., 2016)

In a study by Alberti et al. (2017), flexural and uniaxial fracture tests were carried out on four types of self-compacted concrete mixtures (Table 2.7.). Three-point bending

tests were performed according to RILEM TC-187-SOC on three specimens with 430x100x100 mm in dimension. Specimens were notched with a water cooled low-speed diamond cutting disc. Figure 2.17. presents average load-deflection curves of each mixture. In the figure, the curve P4.5 + S26 gives an algebraic theoretical addition of the responses of P4.5 and S26. When compared with the hybrid H1 behavior, it can be seen that theoretical P4.5+S26 mixture had a smaller toughness. Thus, it can be said that synergetic effect took place between steel and polyolefin fibers in these mixtures.

Table 2.7. Mix design proportions
(Source: Alberti et al., 2017)

	REF	P4.5	S26	H1
Cement (kg/m ³)	375	375	375	375
Limestone powder (kg/m ³)	200	200	200	200
Superplasticizer	1.25% (CEM)	1.25% (CEM)	1.25% (CEM)	1.25% (CEM)
Water (kg/m ³)	187.5	187.5	187.5	187.5
Sand (kg/m ³)	918	918	918	918
Grit (kg/m ³)	245	245	245	245
Gravel (kg/m ³)	367	367	367	367
Polyolefin fibres (kg/m ³)	-	4.5	-	4.5
Steel fibres (kg/m ³)	-	-	26	26

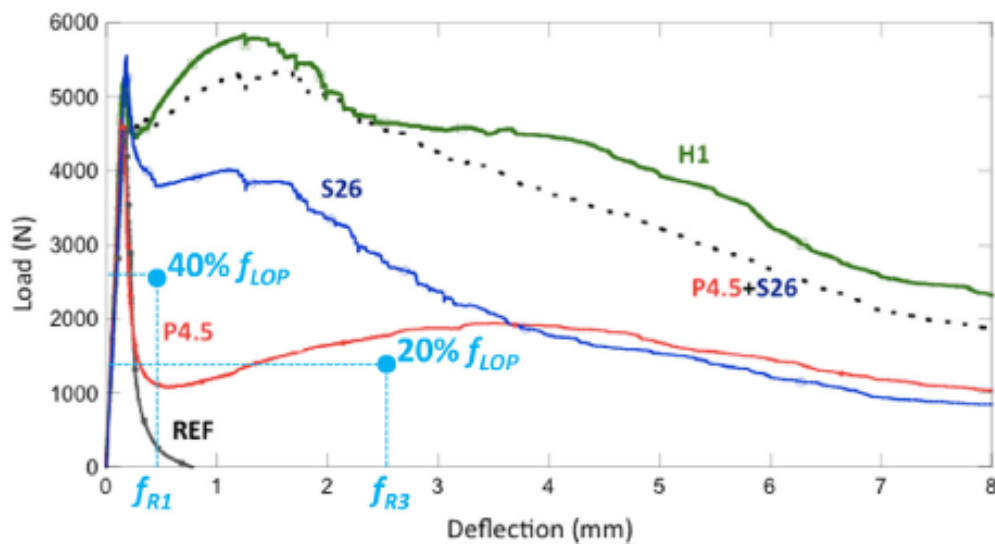


Figure 2.17. Fracture test results: average curve of three specimens of each concrete type (Source: Alberti et al., 2017)

Alberti et al., (2017) performed uniaxial tension tests also on notched specimens by fixing their both ends for rotation. A prismatic specimen of 185x100x100 mm was preferred for uniaxial test and the notch depths were 20 mm. Tests were conducted at a 0.005 mm/min displacement rate.

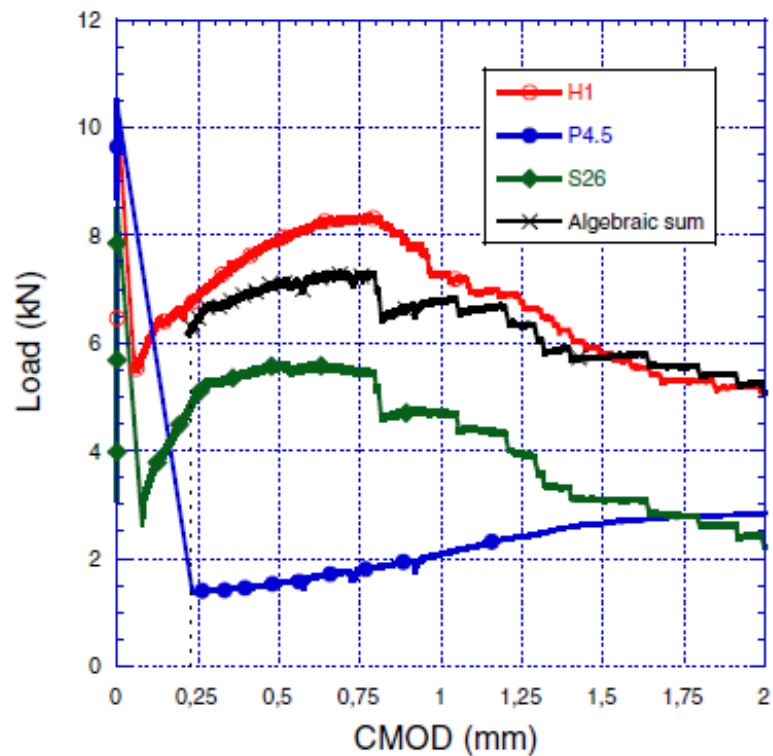


Figure 2.18. Uniaxial test result: average curves of two specimens of each concrete type (Source: Alberti et al., 2017)

Load-CMOD curves for the specimens are presented in Figure 2.18. As it is seen in the figure, S26 and H1 had a similar post-peak slope which means that polyolefin fibers did not contribute to the stiffness of the descending part of the hybrid mixture. However, when H1 and theoretical P4.5+S26 curve was compared synergy effect can be seen clearly.

As seen in the literature, there are numerous studies investigating the effects of hybridization of fibers. Direct tension and bending tests were used in general for this purpose and various synthetic and steel fiber types were tried. Although majority of the studies reported a positive effect when short synthetic and long steel fibers were mixed, there were also studies reporting a negative effect under some circumstances. The study presented here is based on the mix designs and fiber types determined in a previous study by Alami et al., (2018), details of which were mentioned above. HyFRC mix designs determined to give optimal bending performance by Alami et al., (2018) were chosen to be tested under direct tension. In addition, mixes with only steel fibers were also tested and compared with their counterpart steel and PVA fiber HyFRC mixes. In this way, effects of adding PVA fibers to steel fiber mix were investigated in terms of steel fiber type and ratio under direct tension. It has to be noted that majority of studies in the

literature aimed keeping a constant fiber ratio when investigating the effects of hybridization. Such studies obtain HyFRC by replacing part of steel fibers with synthetic fiber. This study, on the other hand, follows an infrequent approach and takes the steel fiber reinforced concrete as the base and examines the effects of adding PVA, which increase the total fiber ratio. As a result, effects of additional PVA fibers could be observed.

CHAPTER 3

EXPERIMENTAL PROGRAM

An extensive experimental program was conducted to investigate the effects of hybridization in fiber reinforced concrete. This chapter presents the details of the materials used, mix design of specimens, and direct tension tests of the specimens. Preliminary tests to determine the specimen geometry and test setup are also described.

3.1. Materials

The materials used in the experimental studies are described below.

Cement: Portland cement (PC), CEM I 42.5 R, in accordance with TS EN 197-1: 2012 was used in all mixtures. The cement had a specific gravity of 3,06. This cement was preferred since it did not contain any fly ash, so that the fly ash content could be controlled in the mixture.

Fly ash: Class-F fly ash in accordance with ASTM C 618 was used with a specific gravity of 2,61.

Aggregates: Crushed limestone was used as coarse aggregate. Aggregate was sieved to obtain a maximum aggregate size of 12 mm. River sand was used as fine aggregate.

48% fine aggregate and 52% coarse aggregate was used in all mixes, according to trials performed in a previous study by Alami et al., (2018). Absorption capacities and specific gravity of coarse and fine aggregates are given in Table 3.1.

Table 3.1. Specific gravity and absorption capacity of fine and coarse aggregates

	Fine aggregate	Coarse aggregate
Specific gravity	2.59	2.56
Absorption capacity (%)	2.67	1.37

Superplasticizer: The superplasticizer was used for obtaining sufficient workability. In this research, polycarboxylate based superplasticizer (MGlenium SKY 608) was used. The admixture is classified as type F according to ASTM C 494/ C 494M 38. Superplasticizer properties are given in Table 3.2.

Table 3.2. Properties of the superplasticizer

Type	Polycarboxylic-based
Color	Opaque
Density	1.063-1.103 kg / liter
Chlorine content	< 0.1 %
Alkali content	< 3 %
Recommended dosage	About 1% of cement content

Synthetic Fibers: Polyvinyl alcohol (PVA) fibers were used in HyFRC mixture. Fibers used were Kuralon K-II RECS 15/8mm brand. The mechanical and geometric properties of PVA fibers are given in Table 3.3.

Table 3.3. Mechanical properties of PVA

Fiber	Length (mm)	Diameter (μm)	Specific Gravity	Nominal Strength (MPa)	Apparent Strength (MPa)	Strain (%)	Young Modulus (GPa)
PVA	8	40	1.3	1610	1092	6	42.8

Steel Fibers: In this study three types of hooked-end Bekaert brand Dramix® steel fibers were used, which were named as 45/35 3D, 65/60 3D and 65/60 5D. Properties of these fibers are given in Table 3.4.

Table 3.4. Mechanical properties of steel fibers

Fiber Type	Aspect Ratio	Length (mm)	Diameter (mm)	Young's Modulus (MPa)	Tensile Strength (MPa)	Hook Geometry
Dramix® 45/35 3D	45	35	0.75	210 000	1225	
Dramix® 65/60 3D	65	60	0.90	210 000	1160	
Dramix® 65/60 5D	65	60	0.90	210 000	2300	

3.2. Mix Design

In this study, four types of mixture were used in the specimens.

- Normal Concrete
- Steel Fiber Reinforced Concrete
- PVA Fiber Reinforced Concrete
- Hybrid Fiber Reinforced Concrete

All mixes had identical cement, water, aggregate and fly ash proportions. Only fiber content was varied.

Normal concrete (NC) was the control mixture without any fibers.

Steel Fiber Reinforced Concrete (SFRC) had only steel fibers in the mix.

PVA Fiber Reinforced Concrete had only PVA fibers in the mix.

Hybrid Fiber Reinforced Concrete (HyFRC) had both steel and PVA fibers in the mix.

The mix design parameters of HyFRC were as follows:

- Binder content = 600 kg/m³
- Fly ash/cement = 1.2
- Three types of steel fibers
- Steel fiber ratio by volume = 0.75% or 1.25%
- PVA ratio by volume = 0.25%

- Maximum coarse aggregate size $D_{max} = 12 \text{ mm}$
- Water/binder = 0.4
- Fine aggregate/coarse aggregate = 48/52

Fiber volume ratios for mixes are given in Table 3.5. The mixes are named according to their content, as “SF-steel fiber type-steel fiber ratio by percentage +PVA (if present)”. For instance, SF45/35_3D_075+PVA defines steel fiber type as 45/35 3D, steel fiber content as 0.75% by volume, and PVA content as 0.25% by volume.

Table 3.5. HyFRC mixture proportions

Mix	Steel Fiber Volume (%)	PVA Fiber Volume (%)
SF45/35_3D_075	0.75	-
SF45/35_3D_075+PVA	0.75	0.25
SF65/60_3D_075	0.75	-
SF65/60_3D_075+PVA	0.75	0.25
SF65/60_5D_075	0.75	-
SF65/60_5D_075+PVA	0.75	0.25
SF65/60_3D_125	1.25	-
SF65/60_3D_125+PVA	1.25	0.25
PVA	-	0.25
Control	-	-

3.3. Tensile Testing of Concrete

Tensile strength of concrete is a significant property in resistance to fracture by bending, freezing and thawing or expansion. There are several methods in the literature for the determination of tensile strength of concrete, such as direct tension tests, split tension tests, three-point bending and four-point bending tests.

The split tension test is a practical test that can be performed on cube-shaped or cylindrical samples (Figure 3.1.). The test is performed by applying compression as a line load on the sample. Principal tensile stresses developing in a direction perpendicular to the principal compression causes tensile cracking in the sample and determines the tensile strength of cementitious composite. Strength obtained from this test is generally greater

than the one obtained from direct tension test and lower than bending tests (ASTM C496/C496M-11).

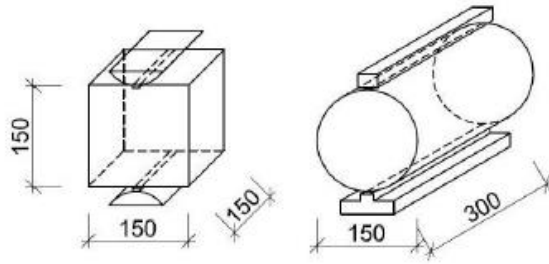


Figure 3.1. Splitting test
(Source: Tipka and Vašková, 2017)

Through bending tests, tensile behavior of steel fiber reinforced concrete is evaluated with load bearing capacity in a certain deflection or crack mouth opening displacement obtained by testing the notched or un-notched beam (RILEM TC 162-TDF, 2002) (Figure 3.2.).

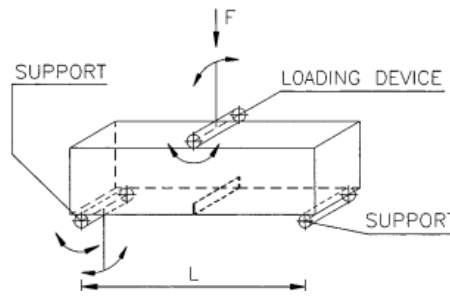


Figure 3.2. Three-point bending test
(Source: RILEM TC 162-TDF, 2002)

In three-point bending tests, the simply supported beam's standard cross-section is 150x150 mm and span is 500 mm. The force is loaded in the middle of span. During test load-central deflection curve is recorded (Figure 3.3.) (RILEM TC 162-TDF, 2002).

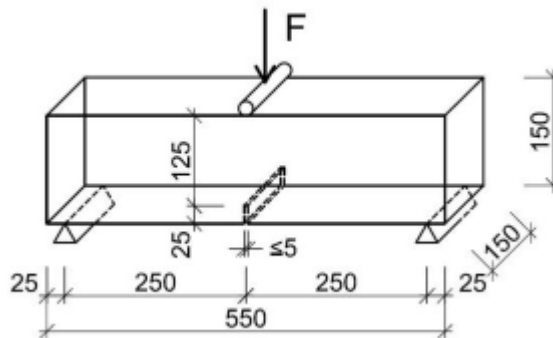


Figure 3.3. Three-point bending test
(Source: Tipka and Vašková, 2017)

Four-point bending test is performed with only un-notched beams. Standard cross-section is 150x150 mm and length is 700 mm. The simply supported beam span is 600 mm and it is loaded with a pair of forces in thirds of span (See Figure 3.4.). During tests, load-central deflection data is recorded (Tipka and Vašková, 2017).

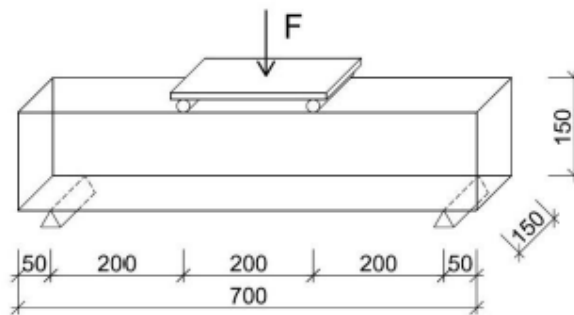


Figure 3.4. Four-point bending test
(Source: Tipka and Vašková, 2017)

Direct tension tests on cylinder specimens are technically more difficult. According to RILEM, the cylindrical specimen diameter is 150 mm and minimum height is 150 mm. The cylinder specimen is notched around whole periphery by 15 mm depth and maximum 5 mm width (Figure 3.5.). There are LVDT sensors for measuring notch mouth opening displacement and control loading. During test, load-crack mouth opening displacement is recorded (Tipka and Vašková, 2017).

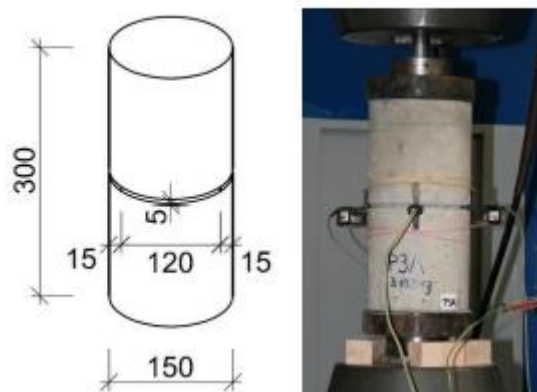


Figure 3.5. Axial tension test - notched cylinder
(Source: Tipka and Vašková, 2017)

Standard tests for bending such as ASTM C1609, JSCE SF-4, and RILEM TC 162-TDF are used to determine the stress-strain of response of fiber reinforced concrete

(FRC). However, there is no standard test for specifying strain-hardening response of concrete in tension (Naaman and Reinhardt, 2006).

Conducting a direct tension test is a challenging work due to the brittle nature of concrete. Difficulties in direct tension tests involve bond failures, bending issues and non-prismatic end regions failures (Van Vliet ,2000). On the other hand, direct tension test is the most suitable test method to determine the post-cracking tension behavior of FRC, since tension is directly introduced on a cross-section without any bending effects like in four-point bending tests and the cracks will have approximately uniform widths which makes it easier to get a relation between crack width and stress. Therefore, direct tension tests are preferred in this study to investigate the synergy effect in FRC.

In direct tension tests, it is recommended to use a cross-section at least twice the length of maximum fiber size, which requires a minimum of 120x120 mm cross section for the fibers used in this study. Such a cross section requires unusually large specimens for direct tension, which makes testing more difficult. Therefore, in this study, a preliminary experimental study was carried out first to determine the proper size and technique to perform these tests. This preliminary study is described in the following section.

3.4. Preliminary Tests

According to literature, there is no standard experimental methodology for determining stress-crack width response of hybrid reinforced concrete in direct tension. Experimental studies in this area involves various specimen geometries and test methods. In this study, a preliminary study was conducted to determine how to perform the direct tension test and to determine optimum sample geometry. Based on literature search, dog-bone geometry for the specimens was found to be advantageous compared to other specimen geometries since failure is initiated at the weakest part of the specimen (Kharal, 2014). Therefore, it was decided to use dog bone shape specimens which were cast in steel molds and had a variable cross section. For these preliminary tests, a geometry recommended by Van Vliet (2000) was used (Figure 3.6.). The sample width was chosen to be 200 mm and other dimensions were calculated accordingly. Keeping the curved parts same, two specimen geometries were tried by leaving a uniform prismatic section in the middle with varying lengths (Figure 3.7.).

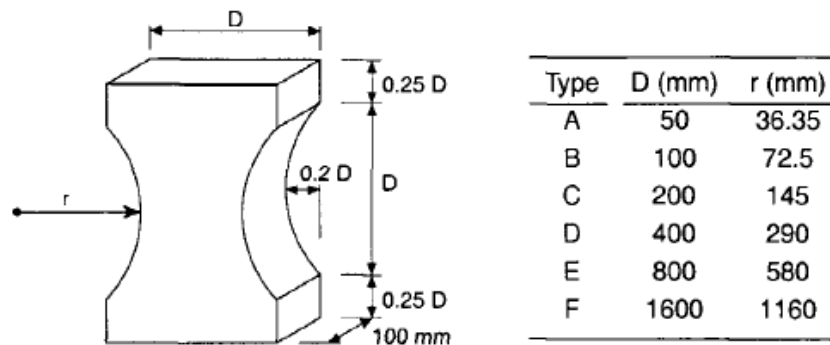


Figure 3.6. Specimen shape and dimensions for adopted size range
(Source: Van Vliet ,2000)

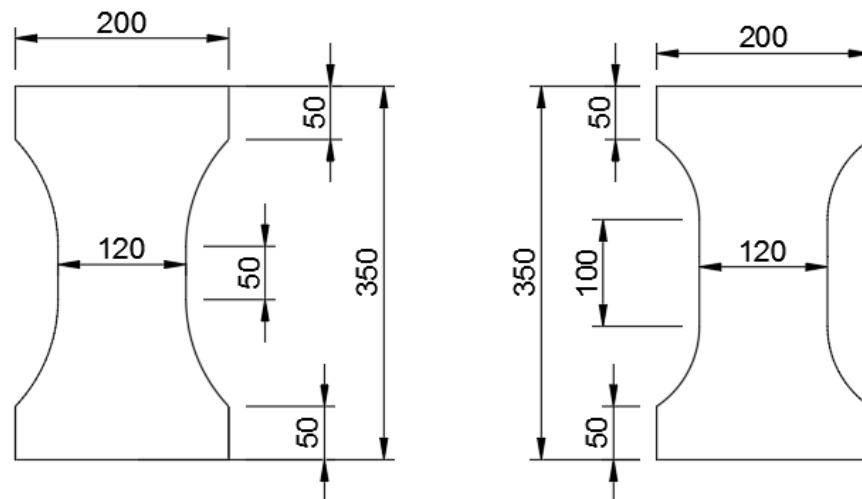


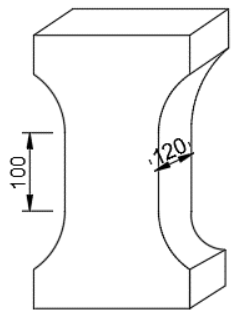
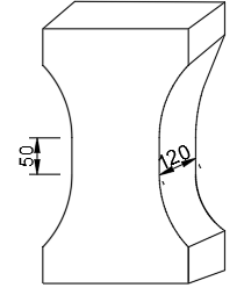
Figure 3.7. Preliminary test specimen geometry

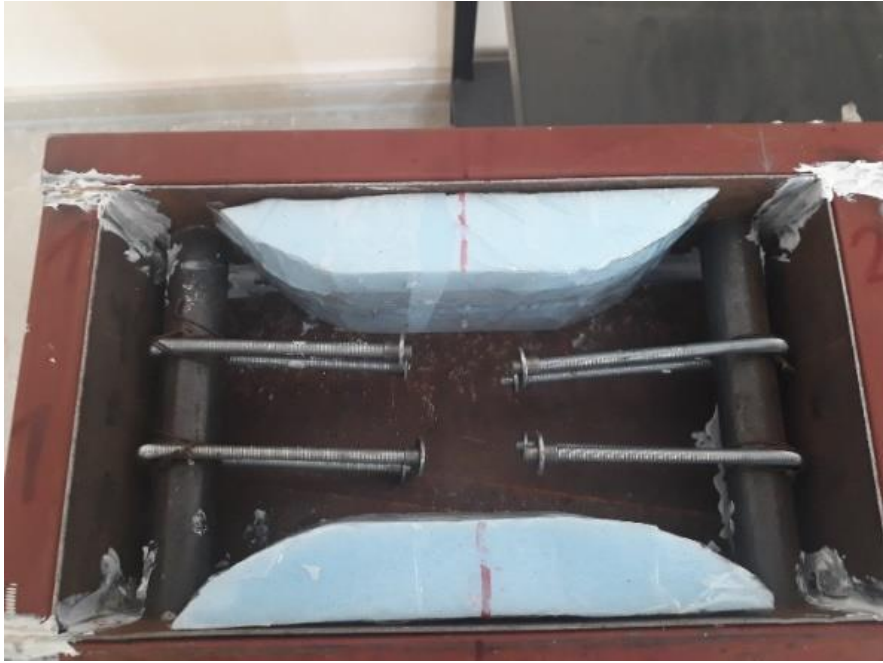
In the specimen geometry, minimum cross-sectional area is at the middle where first cracking is expected to occur. To fix the specimen to the test setup and avoid stress concentration and pullout failure in parts other than the middle of the specimen, some methods were employed.

As the behavior of the specimens could not be predicted precisely in preliminary tests, specimens with different apparatus were prepared. Steel molds were prepared for specimens with six different systems. Styrofoam was prepared and adhered to the mold with silicone to give the shape of a dog bone to the concrete. 19 mm diameter steel tubes, placed at both ends, were embedded to fix the specimens to the test setup. Two 6 mm cold-formed threaded rods or two 8 mm steel bars were bent to U-shape around the perimeter of steel tubes at each end to fix them into the concrete and transfer the load. Steel bars were welded to the tubes, whereas cold-formed threaded rods were tied to the

tubes with steel wires. End of cold-formed threaded rods were fitted with a flange nut to ensure anchorage. To improve anchorage for 8 mm steel bars, 90° end-hooks or welding of short bars to the end were tried. By means of these bars, stress was transferred to the unbonded portion (free distance), whereby only the concrete carries the tensile load. Naming of the specimens are given in Table 3.6. and views of specimens before casting are given in Figure 3.8.

Table 3.6. Preliminary test specimens

Specimen	Geometry	End Reinforcement
T1		Cold-formed threaded rods with flange nuts
T2		Cold-formed threaded rods with flange nuts
T3		Steel bars
T4		Steel bars
T5		Steel bars
T6		Steel bars



(a) T1 (Cold-formed threaded rods with flange nuts, free distance: 60 mm)



(b) T2 (Cold-formed threaded rods with flange nuts, free distance: 80 mm)



(c) T3 (straight steel bars, free distance: 45 mm)



(d) T4 (hooked steel bars, free distance: 45 mm)



(e) T5 (straight steel bars, free distance: 60 mm)

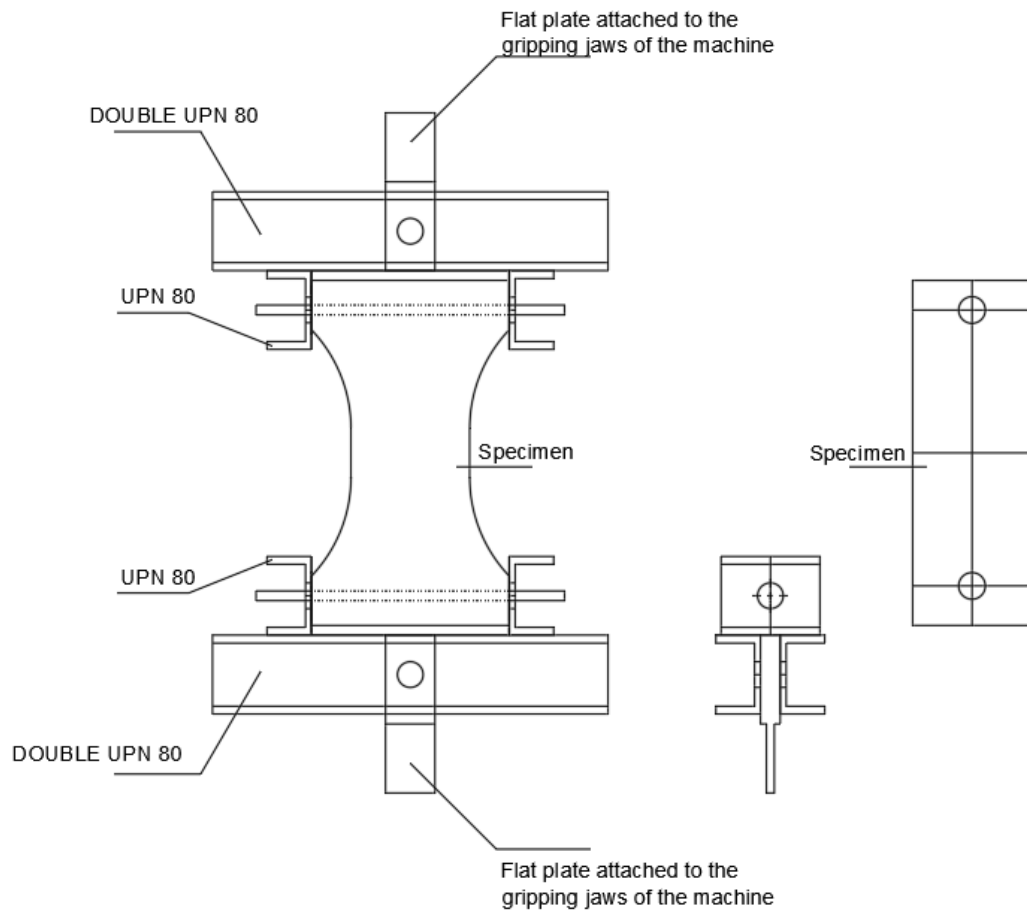


(f) T6 (steel bars with short bars welded at the ends, free distance: 60 mm)

Figure 3.8. Test specimens

After the concrete molds were prepared, all of them were cast with SF65/60_3D_075 mix design, which had 65/60 3D steel fiber with 0.75% volumetric

ratio. A test setup was prepared for the direct tension test that was carried out by a universal testing machine. The experiment setup was designed in a way to provide a hinge system that allowed free rotations at specimen ends. Two UPN 80 profiles were used for mounting a specimen end to test machine. Steel rods were passed through shorter UPN profiles welded on the sides and steel tubes in concrete. A plate holding the UPN's were fixed in the jaw of the machine (Figure 3.9.).



(a) Test Setup



(b) View during testing

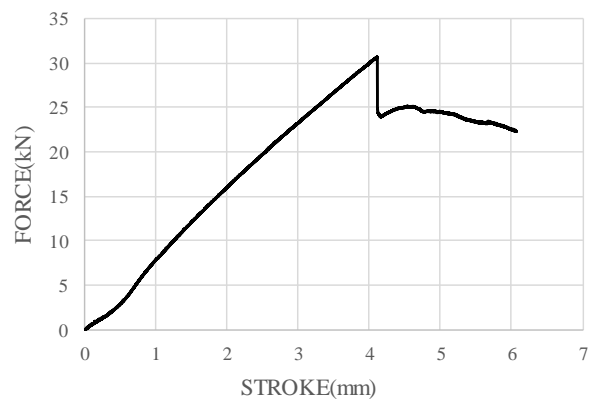
Figure 3.9. Test setup preliminary studies

A displacement-controlled loading was given at 0.5 mm/min rate for all tests.

In T1, a horizontal crack was observed on the front face of the specimen at the straight zone (Figure 3.10.). The maximum tensile load was 30 kN. The crack was observed to widen only on the front face, indicating an eccentricity of load on the specimen.



(a) Final view



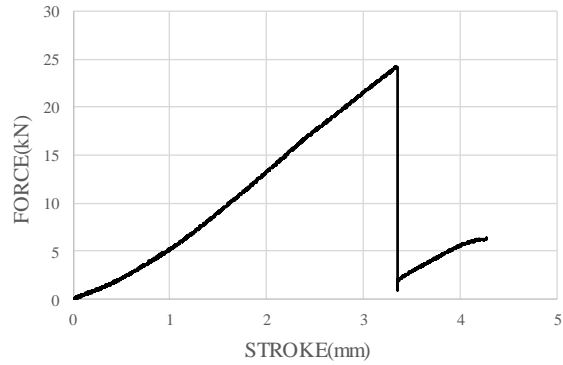
(b) Force-Displacement Curve

Figure 3.10. Test results for T1

In T2, a horizontal crack was developed closer to the top flange of specimen (Figure 3.11.). The maximum tensile load was 24 kN. The crack was observed to widen only on the front face, indicating an eccentricity of load on the specimen.



(a) Final view



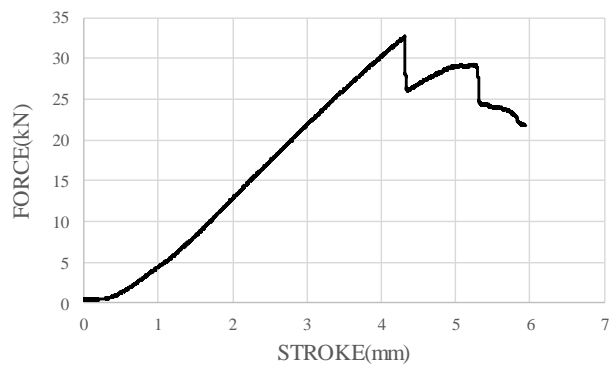
(b) Force-Displacement Curve

Figure 3.11. Test results for T2

In T3, multiple cracking occurred (Figure 3.12.). The maximum tensile load was 32 kN.



(a) Final view



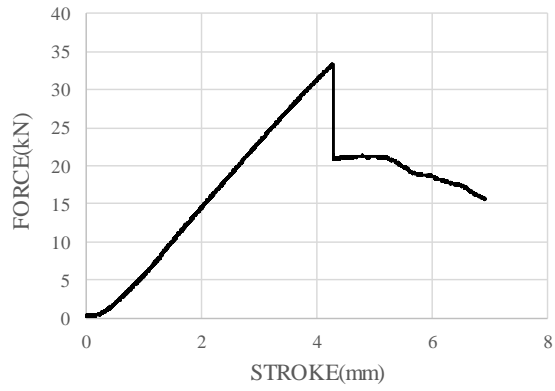
(b) Force-Displacement Curve

Figure 3.12. Test results for T3

T4 showed a very similar behavior to T3 (Figure 3.13.).



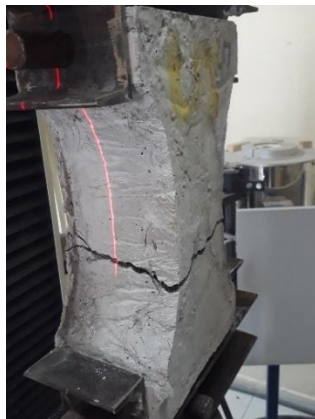
(a) Final view



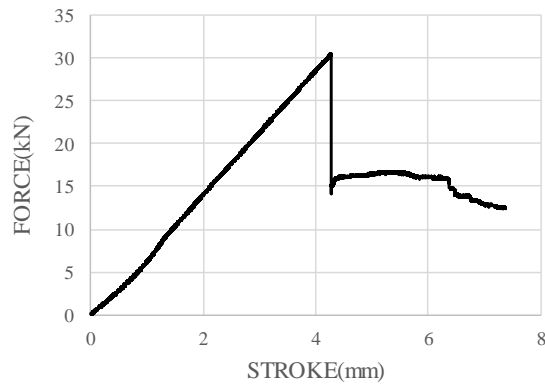
(b) Force-Displacement Curve

Figure 3.13. Test results for T4

In T5, a cracking occurred closer to bottom flange of the specimen (Figure 3.14.). The maximum tensile load was 31 kN. The crack was not horizontal. T6 also gave very similar results. (Figure 3.15.).



(a) Final view



(b) Force-Displacement Curve

Figure 3.14. Test results for T5

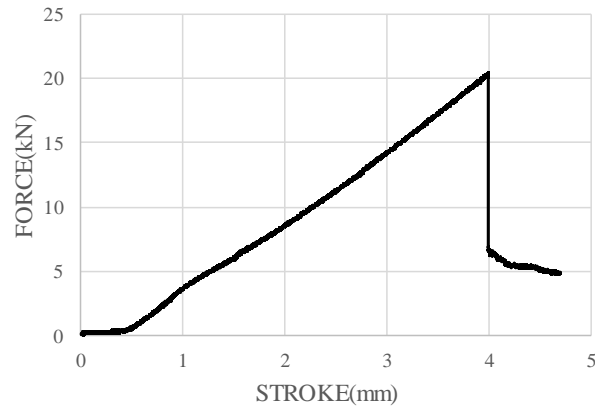


Figure 3.15. Force-displacement curve for T6

The results obtained at the end of the preliminary tests are as follows:

- Cracks in the middle section depend on the way of steel rod anchorages placed in the concrete.
- Craftsmanship was a problem. Even small irregularities in placing the rods caused random cracks in concrete by disturbing the distribution of the load under tension and preventing the spread of the load properly.
- Since the steel bars in the mechanism could not be connected exactly in parallel and equal length, eccentricity occurred under the tensile load causing unsymmetrical cracks to occur.
- The shape of the specimen was found suitable for the experiment and only minor modifications were needed to determine the optimum geometry.
- Although specimen shape could be used, the mechanism to fix it in the testing machine needed to be modified to exclude the embedded tube.
- Therefore, for actual experiments, some changes were made to the shape of the specimen and an appropriate apparatus was designed to fix it in the testing machine.

3.5. Direct Tension Tests

3.5.1. Test Specimen Geometry

According to preliminary studies for direct tension testing, a new dog bone type specimen was designed. Final specimen dimensions are given in Figure 3.16. A notch in

all four sides was cut with a circular hand saw at the mid-height of the specimen to ensure cracking of specimen at the prismatic section. Average notch depth was approximately 7 mm in SF45/35_3D_075, SF45/35_3D_075+PVA, SF65/60_3D_075 and SF65/60_3D_075+ PVA from all sides. In SF65/60_5D_075, SF65/60_5D_075+PVA, SF65/60_3D_125 and SF65/60_3D_125+PVA average notch depth was approximately 11 mm from all sides. In PVA and control group notch depth was approximately 4 mm from all sides. Final notch depth was measured with an electronic caliper for each specimen to obtain the net cross-sectional area.

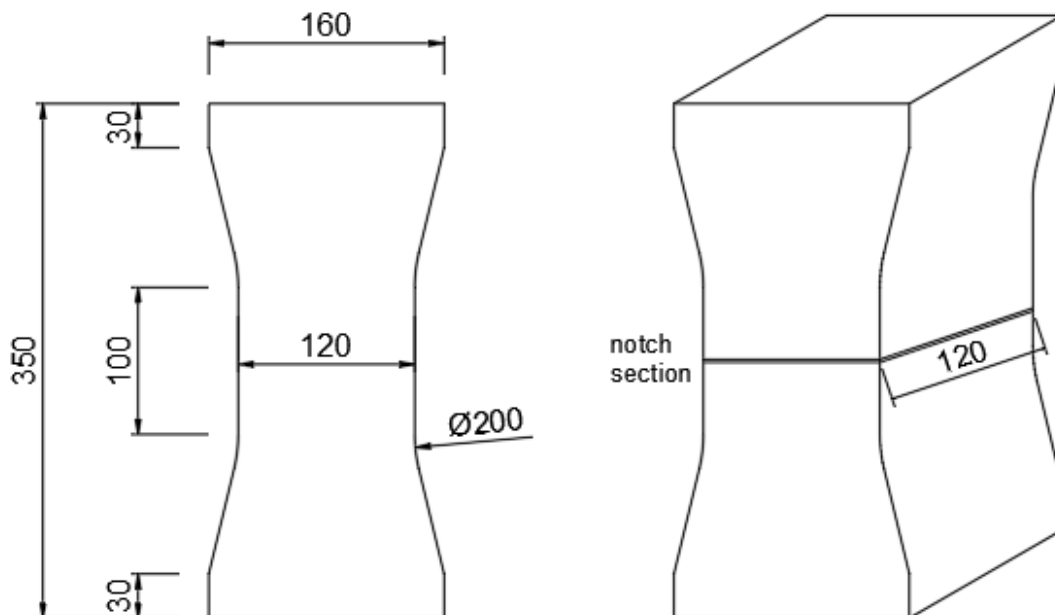


Figure 3.16. Specimen cross section (dimensions are mm)

3.5.2. Preparation of Wooden Molds

Wooden molds for concrete casting were prepared. To obtain the shape of the specimen, stencils were formed from styrofoam and placed in the wooden mold (Figure 3.17.).



Figure 3.17. Wood mold

3.5.3. Mixing Procedure, Casting and Curing

Weight of each material with respect to mix design of concrete was measured. These materials were Portland cement, fly ash, PVA fibers, steel fibers, superplasticizer, fine aggregate and coarse aggregate.

After moisture correction for aggregates, rotating drum mixer with 100 Liter capacity was used for mixing (Figure 3.18.).



Figure 3.18. Rotating drum mixer

Five specimens were cast from each different mix. Specimens that had identical concrete mix were cast all at once using the same batch. Mixing procedure was as follows.

- Sand was introduced into the mixer and mixed for about 1 minute.
- Coarse aggregates were added into mixer and mixed for about 1 minute.
- 2/3 of water was added into mixer and mixed for about 1 minute.
- Portland cement and fly ash were added into mixer and mixed for about 2 minutes.
- Superplasticizer was diluted with remaining water, added into mixer and mixed for about 4 minutes.
- Steel fibers were added into mixer and mixed for about 2 minutes.
- PVA fibers were added into mixer and mixed for about 5 minutes.

For SFRC, PVA FRC and normal concrete same procedure was followed.

- Mixtures were filled to wooden molds and compacted with a tamping rod. Their surface were leveled with a trowel.
- Standard cylindrical specimens of 100 mm diameter and 200 mm height were also cast. During the placing concrete into steel cylinder molds, mixture was compacted with the aid of a tamping rod. Then, the surface of the specimens were levelled.
- Specimens were left in the mold for one day and they were covered with plastic sheets for curing.
- Specimens were removed from molds the following day and they were stored in curing bath until the day of testing (28 days).

3.5.4. Direct Tension Test Setup

Direct tension specimens were tested using a specifically designed test setup with a universal testing machine in İzmir Institute of Technology. The test setup involved UPN 80 profiles attached to the gripping jaws of the testing machine through a pin which allows free rotations (Figure 3.19.). Gripping jaws of the machine had also a limited rotation capacity. The specimen was attached to this assembly with hand-tightened screws. 10 mm thick steel plates were placed on the specimen at the attachment points to allow for a uniform contact stress distribution. Contact surface of these plates were also leveled with

gypsum for a perfect contact. With this system, tension force applied by the machine was transferred to the UPN profiles through the pin. UPN profiles transferred the force on the specimen through the locking system created by the screws.

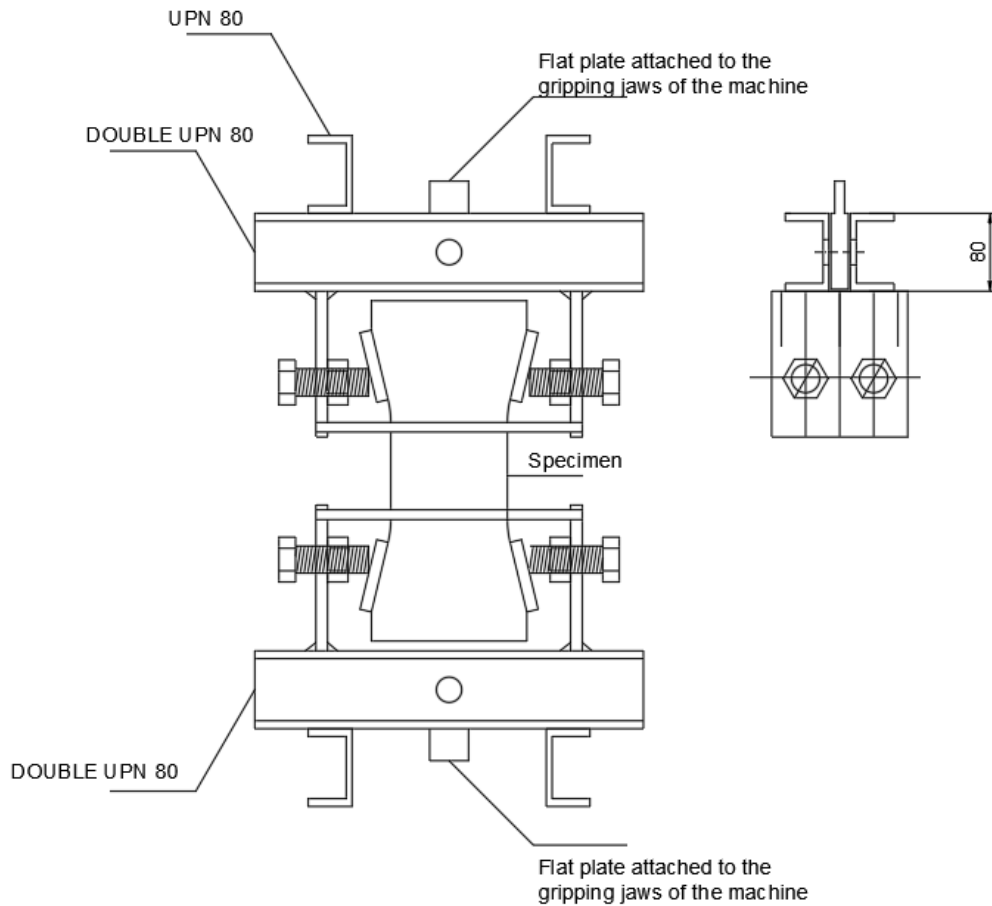


Figure 3.19. Test setup drawing

A displacement-controlled loading was applied at a 0.3 mm/minute loading rate. Tensile force on the specimen and the stroke was measured with the load cell and displacement transducer of the testing machine (Figure 3.20. and Figure 3.21.). Crack width was measured both manually and with a video extensometer. Video extensometer measured the change in distance between two stickers placed approximately 10 mm apart on top and bottom sides of the cut notch. Video extensometer was found to be unreliable for large displacements, so the crack width was also measured manually using a digital movement gage (Figure 3.22.). During testing, after first cracking was observed, this gage was used to manually measure distances between beads attached on the specimen.

These beads were placed in four pairs, for each pair one at the top and one at the bottom of the notch, approximately 40 mm apart (Figure 3.23.). Two pairs were attached each on the front and rear face of the specimen 15 mm close to the corners. Original distance between beads were measured before testing. Load was paused after cracking for approximately every 0.5 mm stroke and change in distance between beads were measured manually and recorded (Figure 3.24.). Average of four recordings obtained from each pair located close to corners gave the average crack width. By this way, unsymmetrical crack opening was also taken into consideration. After each test, these recordings were correlated with the measured stroke. For all specimens, strong correlation was found between the crack width and stroke (Figure 3.25.). Therefore, for following crack width-stress calculations, this correlation was used to obtain crack width using stroke, which was automatically recorded for every 0.05 seconds.



Figure 3.20. Test specimen



Figure 3.21. Test setup



Figure 3.22. Digital movement gauge



Figure 3.23. Test specimen

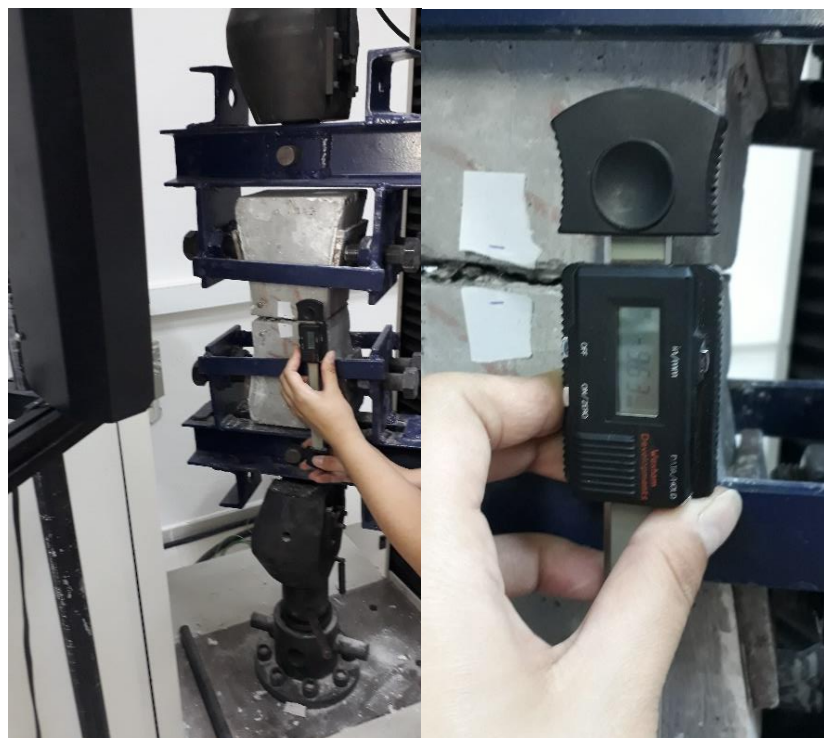


Figure 3.24. Measuring manually

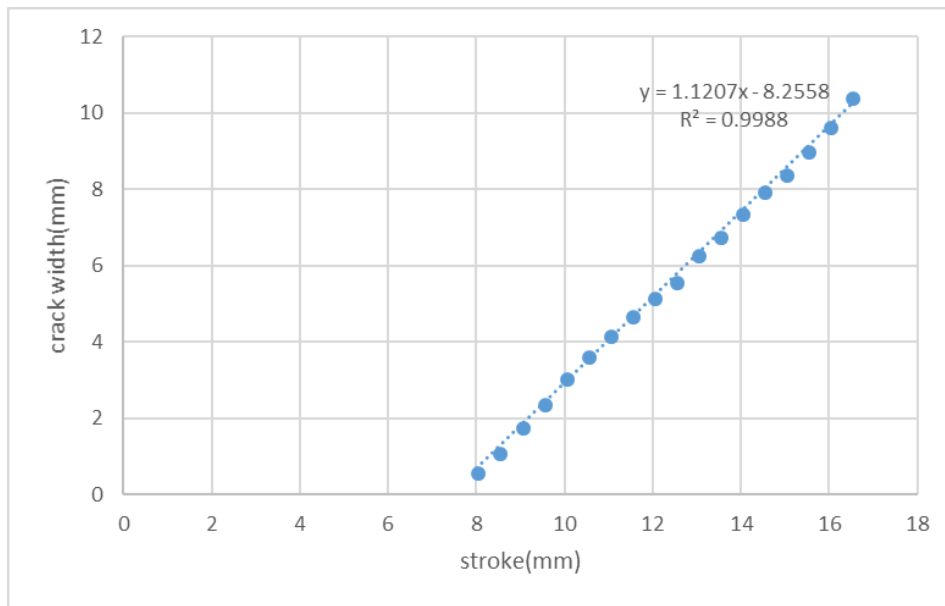


Figure 3.25. Avg crack width- stroke graph

3.5.5. Compressive Strength Test

Three cylindrical specimens were cast for each mixture compressive strength test. Cylinder specimens were 200 mm in length and 100 mm in diameter. These specimens were tested according to ASTM C 39, Standard Test Method for Compressive Strength of Cylindrical Concrete Specimens, 28 days after casting. All cylinder specimens were capped with gypsum to ensure a uniform load distribution at the ends (Figure 3.26.). Compression tests were carried out using a digital compression machine as given in Figure 3.27. Load controlled test speed was 0.6 N/mm²s.



Figure 3.26. Cylinder specimens



Figure 3.27. Digital compressive test machine

CHAPTER 4

RESULTS AND DISCUSSIONS

4.1. Compressive Strength Test Results

Table 4.1. presents the compressive strength tests results for mixtures at 28 days. During concrete casting, three cylinder specimens were taken for each mixtures. Results shown in the table are the average values of three test results. For control group, six specimens were cast and tested.

Table 4.1. Compressive strength test results

Mix	Compressive Strength (MPa)
SF45/35_3D_075	35.33
SF45/35_3D_075+PVA	30.89
SF65/60_3D_075	30.02
SF65/60_3D_075+PVA	31.04
SF65/60_5D_075	32.20
SF65/60_5D_075+PVA	27.67
SF65/60_3D_125	29.01
SF65/60_3D_125+PVA	26.52
PVA	31.29
Control	31.03

The Table 4.1. shows that compressive strength results for all mixtures with fiber and without fiber. The control group's concrete compressive strength was around 31.03 MPa. According to test results, adding PVA fiber increased compressive strength to 31.29 MPa. It was observed that the addition of low volume percentage PVA fiber increased the compressive strength slightly.

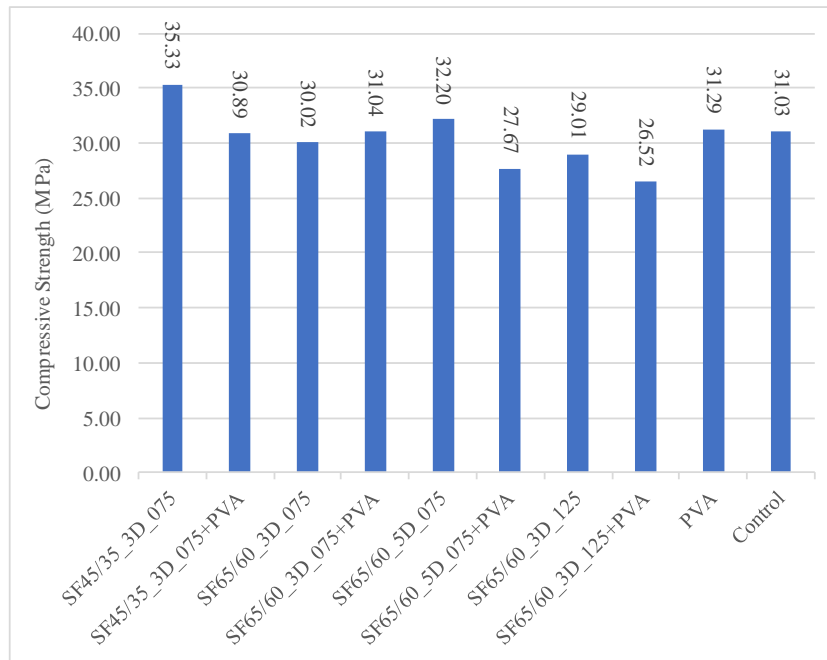


Figure 4.1. Compressive strength test results

The compressive strength of mixes containing only steel fibers ranges from 29.01 to 35.33 whereas mixes containing both steel fiber and PVA fiber ranges from 26.52 to 31.04. Compressive strength of some HyFRC mixtures were higher than only steel fiber mixtures, but some of them were very close or lower. (Figure 4.1.) This is probably a result of low workability and reduced compressive strength in concrete due to clustering of PVA and steel fibers.

4.2. Direct Tension Test Results

Direct tension cracking strength test results are presented in Table 4.2. for all tested specimens. Note that although five specimens were tested for each mix, some of them either cracked unsymmetrically at the notch due to clustering of steel fibers on one side or crushed under compression at the gripping points. Those tests were considered to be invalid and only valid tests that showed a symmetrical cracking at the notch are reported here. To give an idea about the energy consumed by these specimens under tension, area under stress-crack width curves until 10 mm crack width is also calculated and presented in Table 4.2. Energy consumed were not calculated for PVA and Control specimens since these specimens failed suddenly and split into two without sustaining

any tensile stresses after cracking. Following sections discusses the test results obtained from each mix.

Table 4.2. Direct tension test results

Mix		Ultimate Strength (MPa)	Energy Consumed (Nmm/mm ²)
SF45/35_3D_075	1	1.85	7.70
	2	1.15	6.64
	3	2.14	7.47
	Avg	1.53	7.23
	Standard deviation(σ)	0.51	0.55
	Coefficient of variation(cv)	0.33	0.08
	Coefficient of dispersion(cd)	0.29	0.06
SF45/35_3D_075+PVA	1	1.63	6.71
	2	2.04	9.92
	3	1.72	7.17
	Avg	1.80	7.93
	Standard deviation(σ)	0.22	1.73
	Coefficient of variation(cv)	0.12	0.22
	Coefficient of dispersion(cd)	0.09	0.17
SF65/60_3D_075	1	1.85	12.49
	2	1.90	12.93
	Avg	1.88	12.69
	Standard deviation(σ)	0.04	0.31
	Coefficient of variation(cv)	0.02	0.02
	Coefficient of dispersion(cd)	0.01	0.02
SF65/60_3D_075+PVA	1	1.72	16.48
	2	2.35	18.12
	3	1.93	16.01
	Avg	1.97	16.32
	Standard deviation(σ)	0.32	1.11
	Coefficient of variation(cv)	0.16	0.07
	Coefficient of dispersion(cd)	0.11	0.05
SF65/60_5D_075	1	3.02	19.26
	2	3.55	19.92
	3	2.80	17.94
	Avg	3.12	19.04
	Standard deviation(σ)	0.39	1.02
	Coefficient of variation(cv)	0.13	0.05
	Coefficient of dispersion(cd)	0.09	0.04

(cont. on next page)

Table 4.2 (cont.)

SF65/60_5D_075+PVA	1	3.12	19.90
	2	2.70	17.24
	Avg	2.91	18.57
	Standard deviation(σ)	0.30	1.88
	Coefficient of variation(cv)	0.10	0.10
	Coefficient of dispersion(cd)	0.07	0.07
SF65/60_3D_125	1	3.94	28.36
	2	3.36	28.07
	Avg	3.65	28.22
	Standard deviation(σ)	0.41	0.21
	Coefficient of variation(cv)	0.11	0.01
	Coefficient of dispersion(cd)	0.08	0.01
SF65/60_3D_125+PVA	1	3.17	25.27
	2	2.78	26.00
	Avg	2.95	25.64
	Standard deviation(σ)	0.28	0.52
	Coefficient of variation(cv)	0.09	0.02
	Coefficient of dispersion(cd)	0.07	0.01
PVA	1	1.24	-
	2	1.20	-
	3	1.26	-
	4	1.59	-
	5	1.48	-
	Avg	1.35	-
	Standard deviation(σ)	0.17	-
	Coefficient of variation(cv)	0.13	-
	Coefficient of dispersion(cd)	0.11	
Control	1	1.63	-
	2	1.70	-
	3	1.87	-
	4	1.65	-
	Avg	1.71	-
	Standard deviation(σ)	0.11	-
	Coefficient of variation(cv)	0.06	-
	Coefficient of dispersion(cd)	0.05	

Specimens that yielded a valid result were identified by its number following the specimen group name. Figures 4.2 to 4.27 present a view of the specimens after testing

and followed by the stress crack width curve of these specimens. Average of valid stress-crack width curves were also calculated and presented in stress-crack width figures.



Figure 4.2. SF45/35_3D_075-1 specimen after cracking



Figure 4.3. SF45/35_3D_075-2 specimen after cracking



Figure 4.4. SF45/35_3D_075-3 specimen after

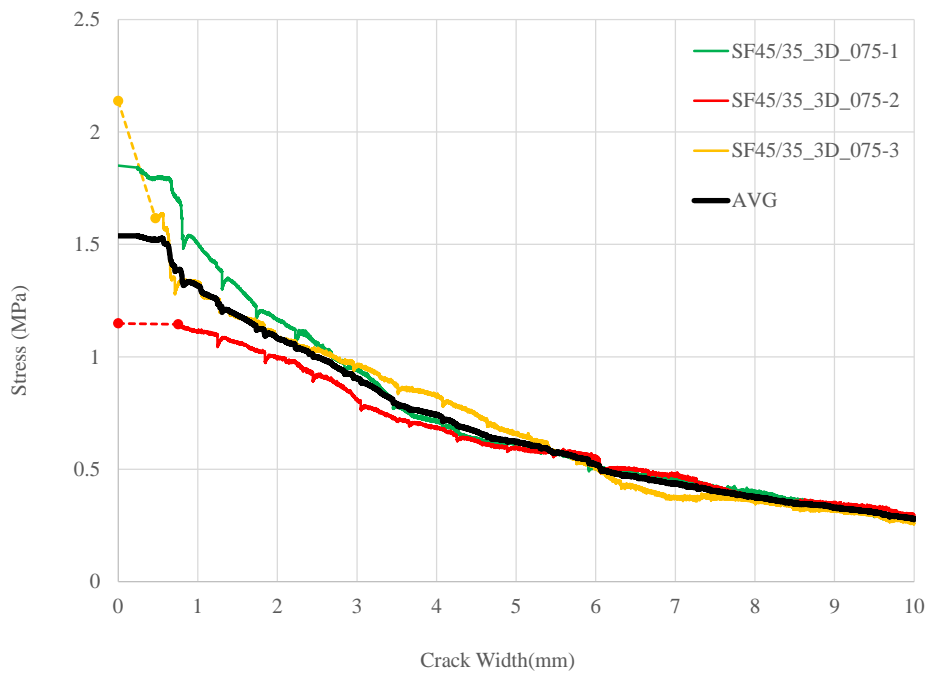


Figure 4.5. Stress-crack width curve for SF45/35_3D_075 (SFRC)



Figure 4.6. SF45/35_3D_075+PVA-1 specimen after cracking



Figure 4.7. SF45/35_3D_075+PVA-2 specimen after cracking



Figure 4.8. SF45/35_3D_075+PVA-3 specimen after cracking

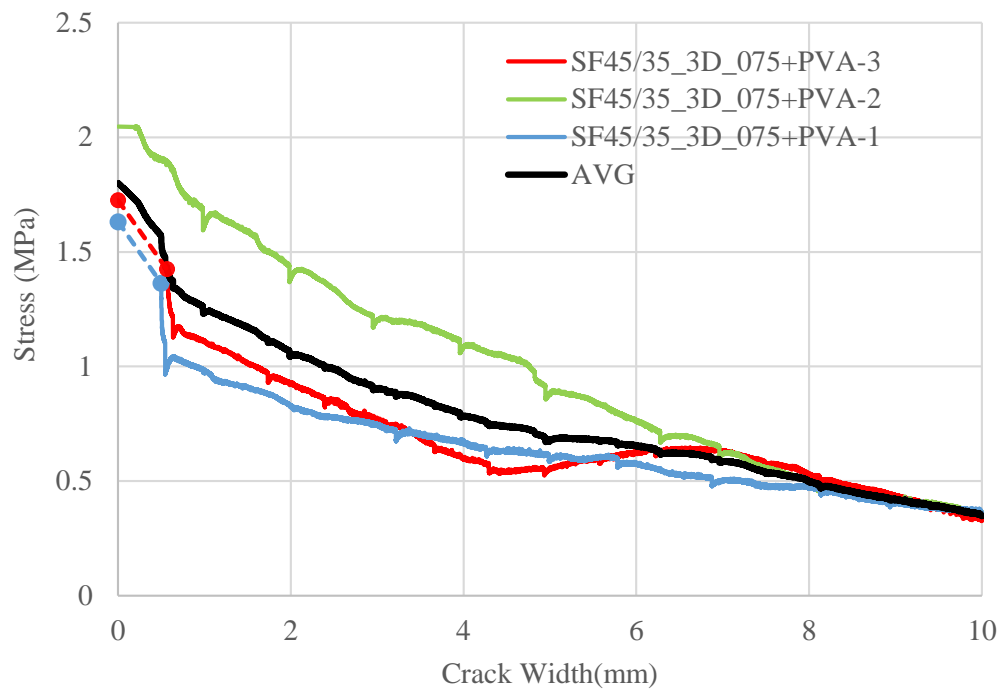


Figure 4.9. Stress-crack width for SF45/35_3D_075+PVA(HyFRC)



Figure 4.10. SF65/60_3D_075-1 specimen after cracking



Figure 4.11. SF65/60_3D_075-2 specimen after cracking

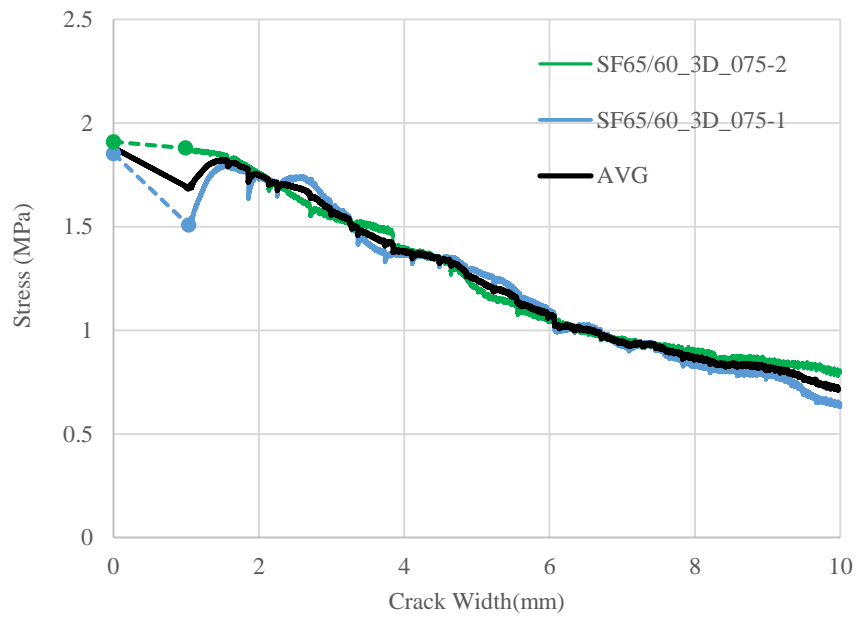


Figure 4.12. Stress-crack width curve for SF65/60_3D_075 (SFRC)



Figure 4.13. SF65/60_3D_075+PVA-2 specimen after cracking



Figure 4.14. SF65/60_3D_075+PVA-3 specimen after cracking

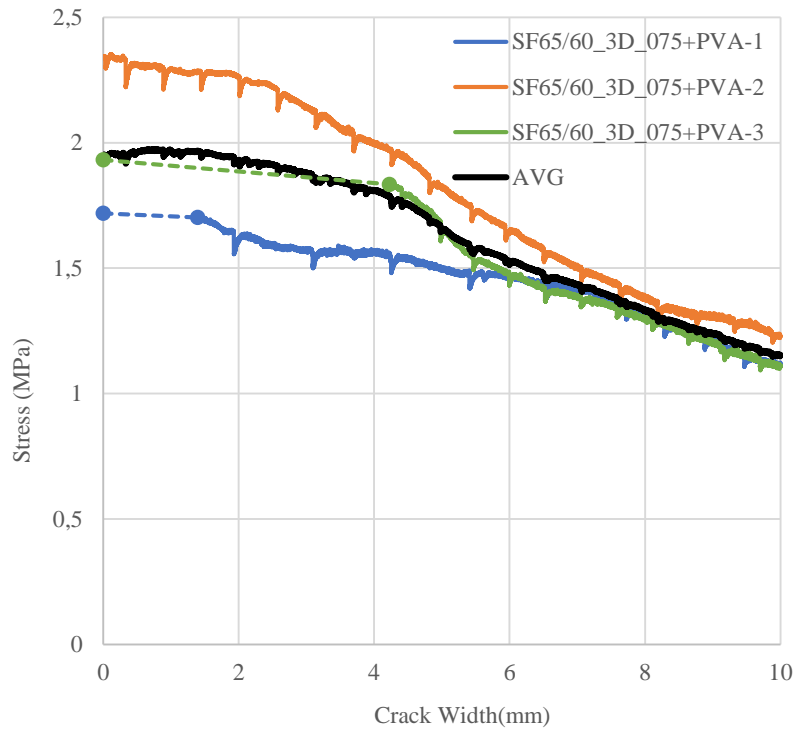


Figure 4.15. Stress–crack width curve for SF65/60_3D_075+PVA (HyFRC)



Figure 4.16. SF65/60_5D_075-1 specimen after cracking



Figure 4.17. SF65/60_5D_075-2 specimen after cracking

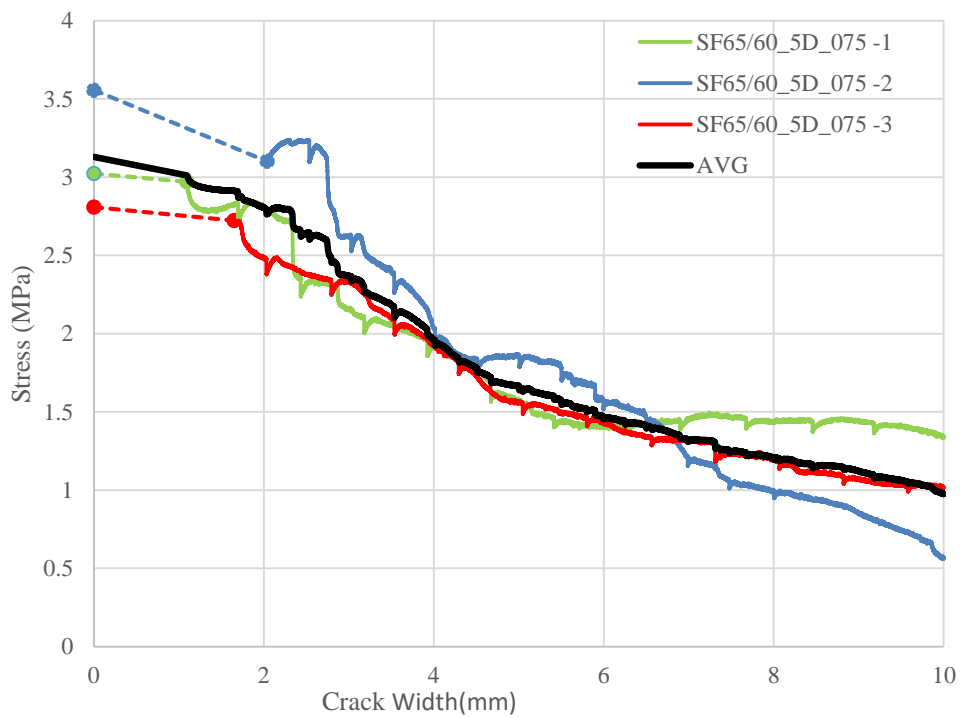


Figure 4.18. Stress-crack width curve for SF65/60_5D_075 (SFRC)



Figure 4.19. SF65/60_5D_075+PVA-2 specimen after cracking



Figure 4.20. SF65/60_5D_075+PVA-3 after cracking

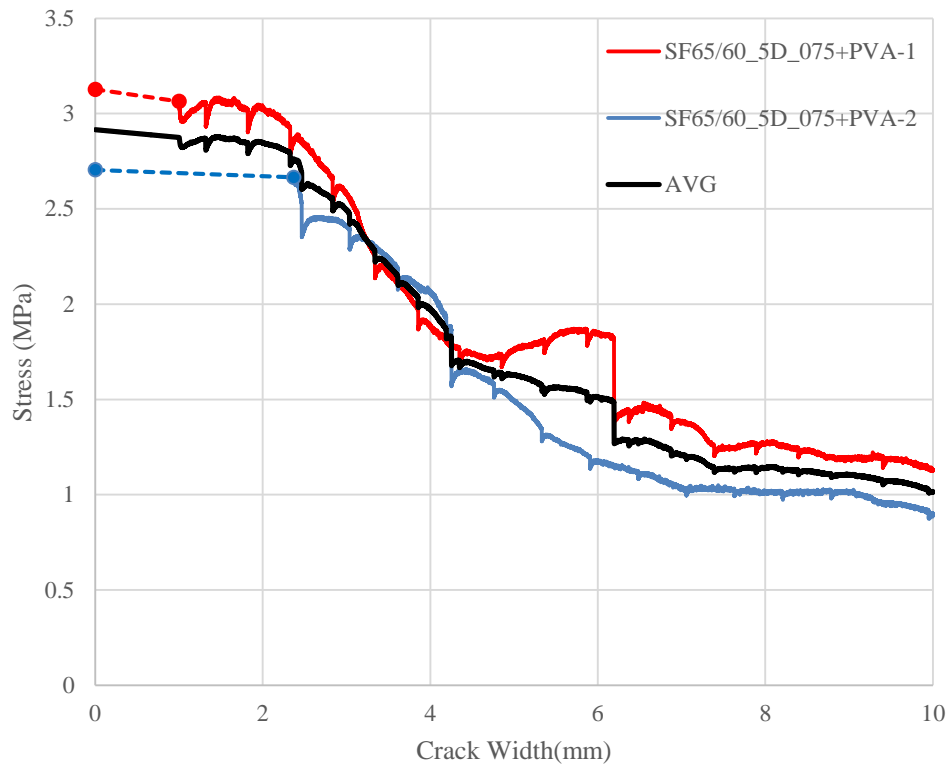


Figure 4.21. Stress-crack width curve for SF65/60_5D_075+PVA (HyFRC)



Figure 4.22. SF65/60_3D_125-1 specimen after cracking

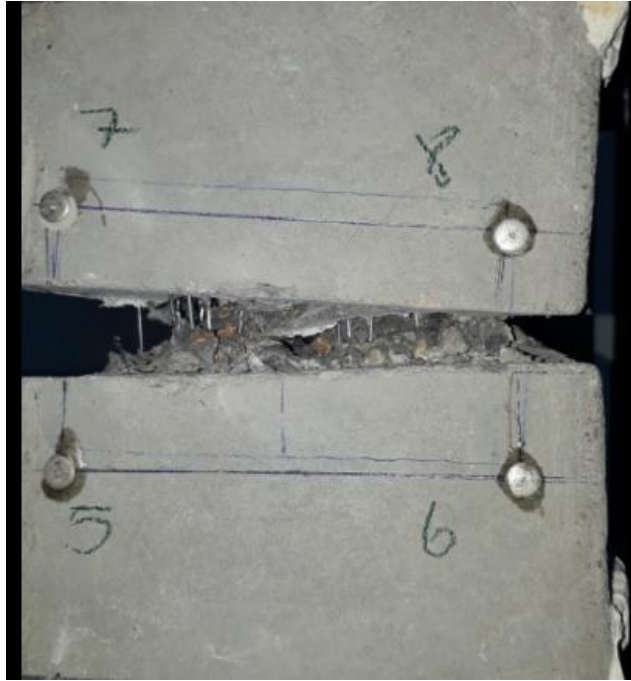


Figure 4.23. SF65/60_3D_125-2 specimen after cracking

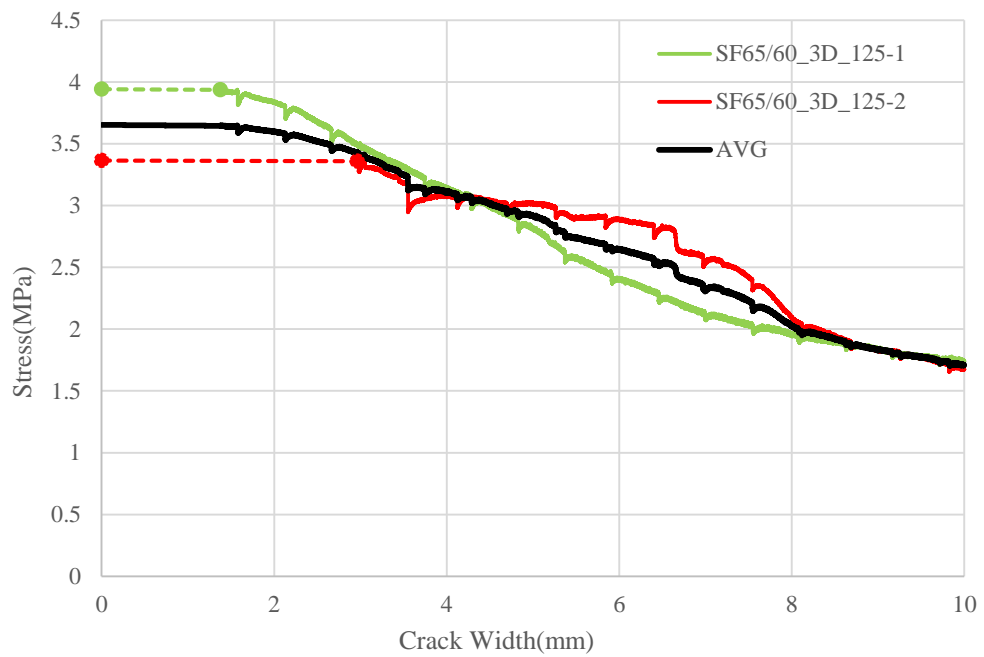


Figure 4.24. Stress-crack width curve for SF65/60_3D_125 (SFRC)



Figure 4.25. SF65/60_3D_125+PVA-1 specimen after cracking



Figure 4.26. SF65/60_3D_125+PVA-2 specimen after cracking

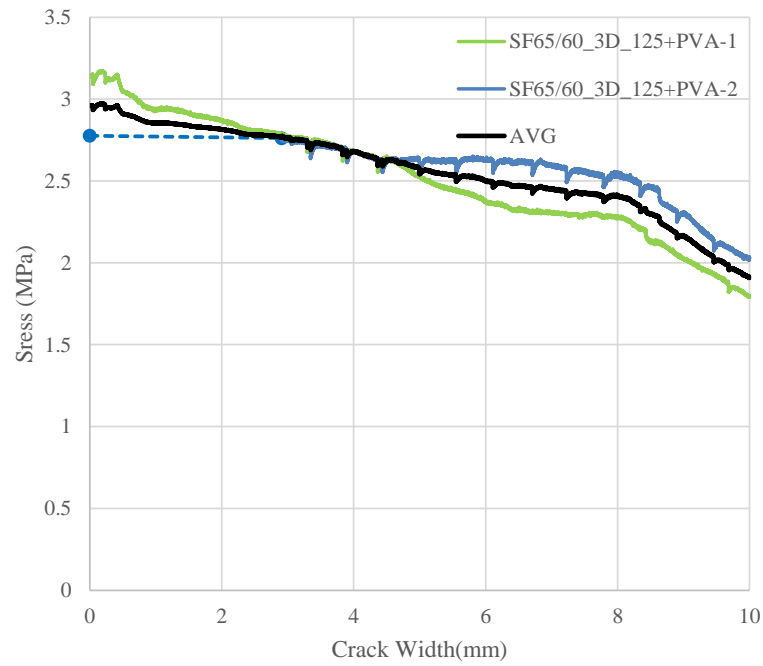


Figure 4.27. Stress-crack width curve for SF65/60_3D_125+PVA (HyFRC)

PVA Group mixture contains only PVA fiber. The PVA fiber content is 0,25% by volume. The five specimens were tested for PVA group. Figures 4.28. to 4.31. present a view of the specimens of PVA and control group after testing.

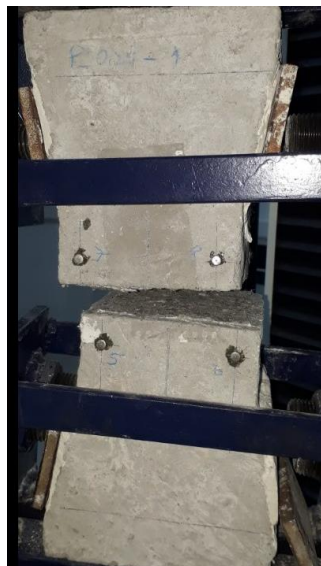


Figure 4.28. PVA group specimen after cracking



Figure 4.29. PVA group specimen after cracking

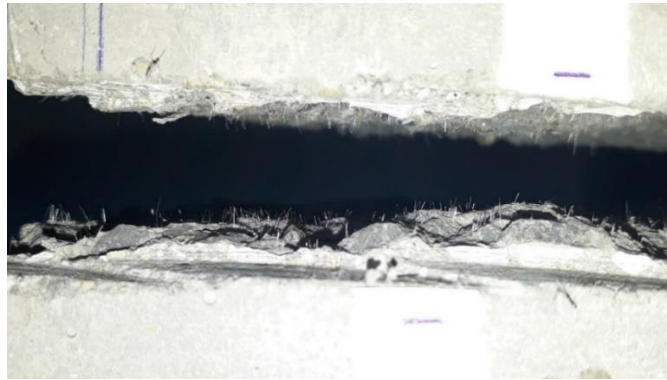


Figure 4.30. PVA group specimen after cracking



Figure 4.31. Normal concrete group specimen after cracking

4.3. Discussion of Direct Tension Test Results

Average tensile cracking strength results are presented in Figure 4.32. Energy consumed by the specimens, calculated as the area under stress-crack width curve until 10 mm crack width, are also presented in Figure 4.33.

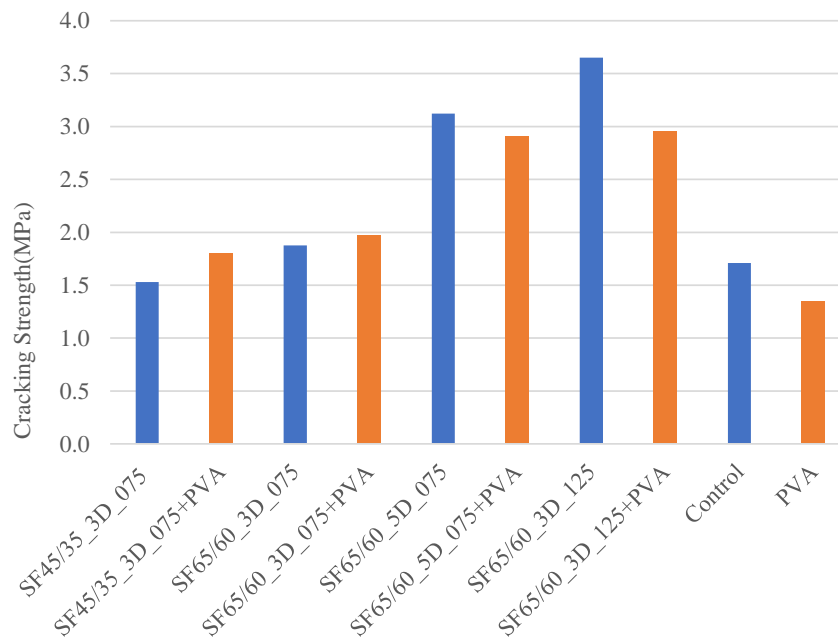


Figure 4.32. Average tensile cracking strength

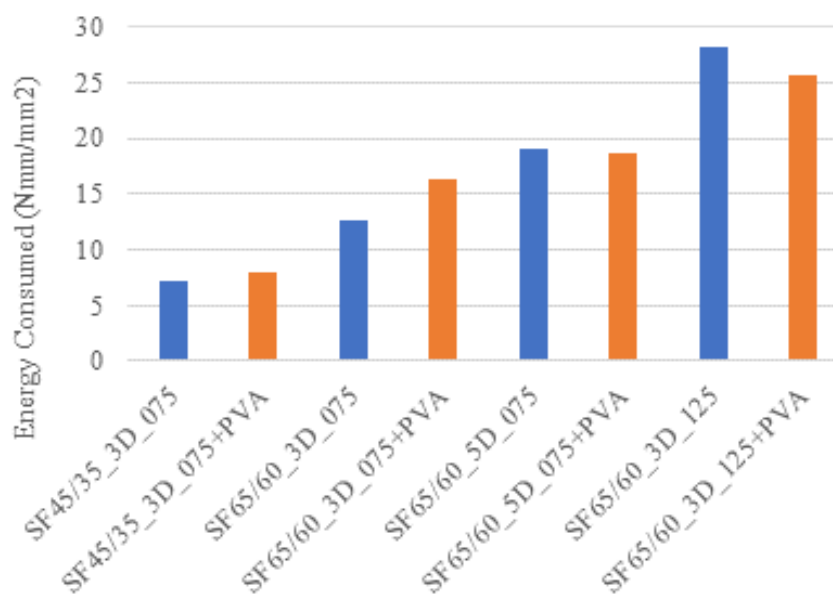


Figure 4.33. Average energy consumed of each mixtures

As seen in Figure 4.32., fiber inclusion increased tensile strength for all specimens compared to control group. The highest tensile strength was obtained in SF65/60_3D_125. The average tensile strength of control group and PVA group specimens were calculated as 1.71 MPa and 1.35 MPa, respectively. In this case, the addition of PVA fiber alone had a decreasing effect on the tensile strength. Both control group and PVA group displayed a sudden cracking that split the specimen into two. Therefore, a stress-crack width response could not be obtained for these groups. Average tensile stress-crack width responses of groups without and with PVA are given in Figures 4.34. and 4.35., respectively.

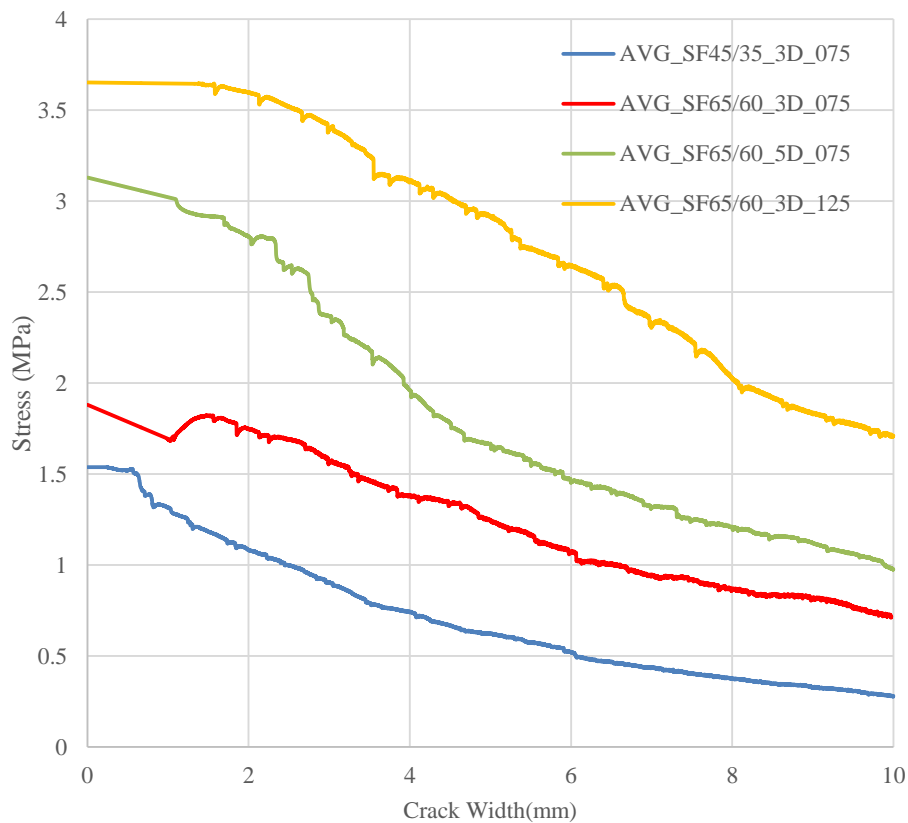


Figure 4.34. Average tensile stress-crack width curves

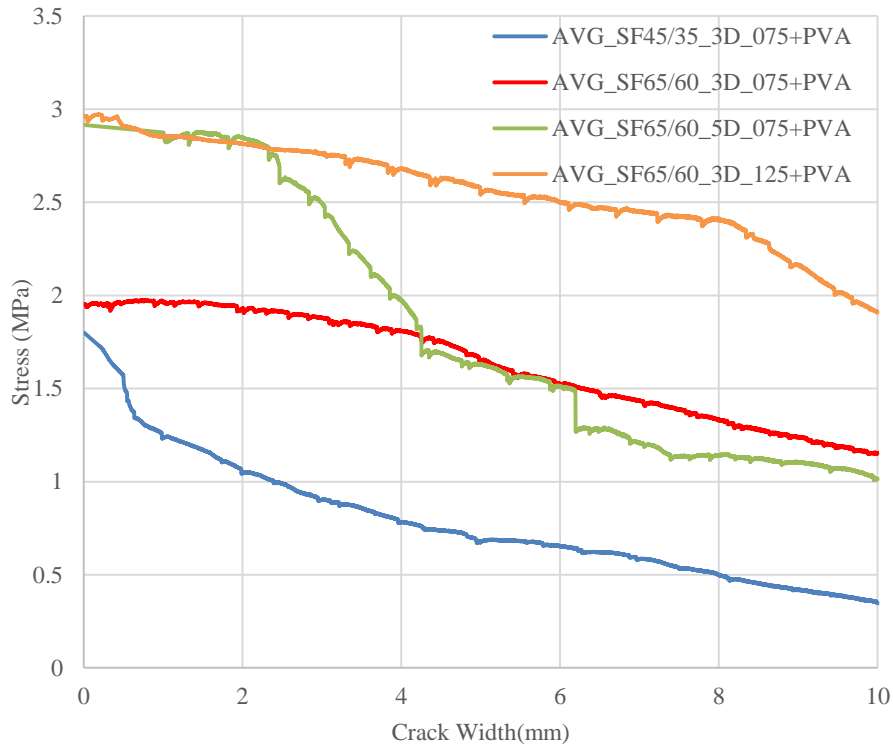


Figure 4.35. Average tensile stress-crack width curves

As seen in Figure 4.34., compared to other mixtures, among the groups that did not have PVA, the mixture that sustained highest level of tensile stresses was SF65/60_3D_125, as a result of higher fiber ratio. Tensile stresses and consumed energies of SF65/60_3D_075 and SF65/60_5D_075 were higher compared to SF45/35_3D_075. The higher aspect ratio and longer length of SF65/60_3D_075 and SF65/60_5D_075 provided greater interfacial bond strength by larger connection area between fiber and matrix. Dramix® 65/60 3D and Dramix® 65/60 5D have identical length and aspect ratio. However, SF65/60_5D_075 sustained higher levels of tensile stresses compared to SF65/60_3D_075 due to double-hook ends that provide better anchorage.

General trend for groups with PVA was similar to the groups without PVA. As seen in Figure 4.35., the mixture that sustained highest level of tensile stresses was SF65/60_3D_125+PVA. With PVA addition, SF65/60_5D_075+PVA was able to reach to tensile stress levels of SF65/60_3D_125+PVA. But for this group, stress levels dropped quickly with widening crack width and dropped to even levels below SF65/60_3D_075+PVA. Therefore, adding PVA to SF65/60_5D_075 did not enhance the behavior to levels that was obtained by higher steel fiber ratio.

Comparisons of test results in terms of effects of adding PVA are presented and discussed in following sections.

4.3.1. SF45/35_3D_075 and SF45/35_3D_075+PVA Mixtures

Average stress-crack width behavior of SF45/35_3D_075 and SF45/35_3D_075+PVA is compared in Figure 4.36. PVA addition increased the cracking stress by about 18% and consumed energy by about 10%. Stress-crack width behavior was similar until about 3 mm crack width. But after 3 mm, SF45/35_3D_075+PVA sustained higher levels of tensile stress and consequently consumed more energy. For this mix, adding PVA enhanced the tension performance of the specimens.

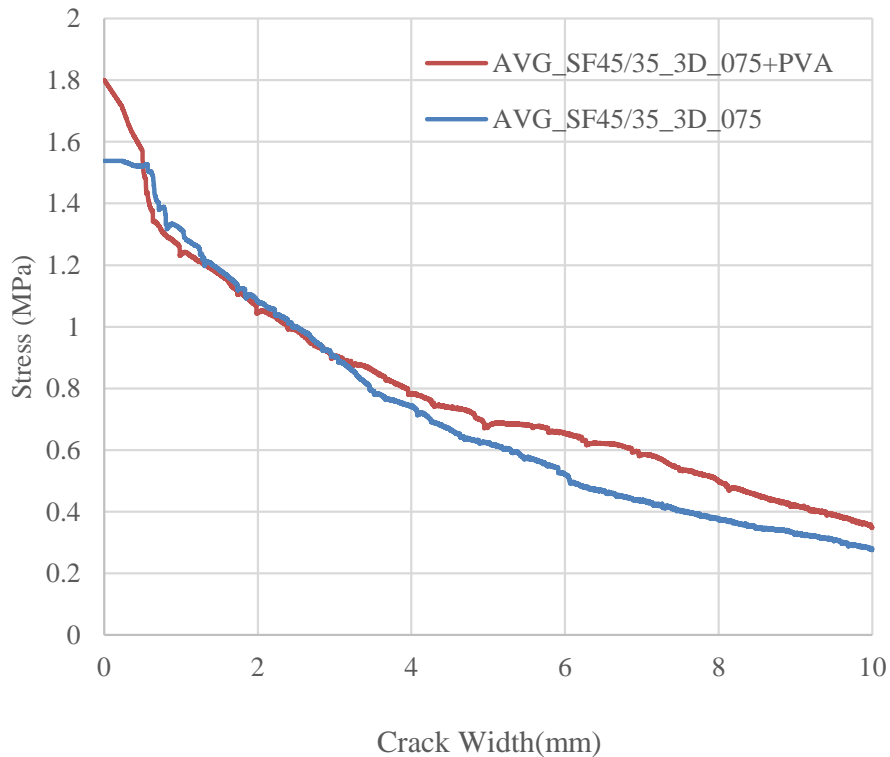


Figure 4.36. Average stress-crack width curves

4.3.2. SF65/60_3D_075 and SF65/60_3D_075+PVA Mixtures

Average stress-crack width behavior of SF65/60_3D_075 and SF65/60_3D_075+PVA is compared in Figure 4.37. PVA addition slightly increased the

cracking stress by about 5%. However, consumed energy increased by about 29%. SF65/60_3D_075+PVA sustained considerable higher tensile stresses compared to SF65/60_3D_075. Although increase in tensile strength was minimal, hybridization significantly enhanced tension behavior for this group.

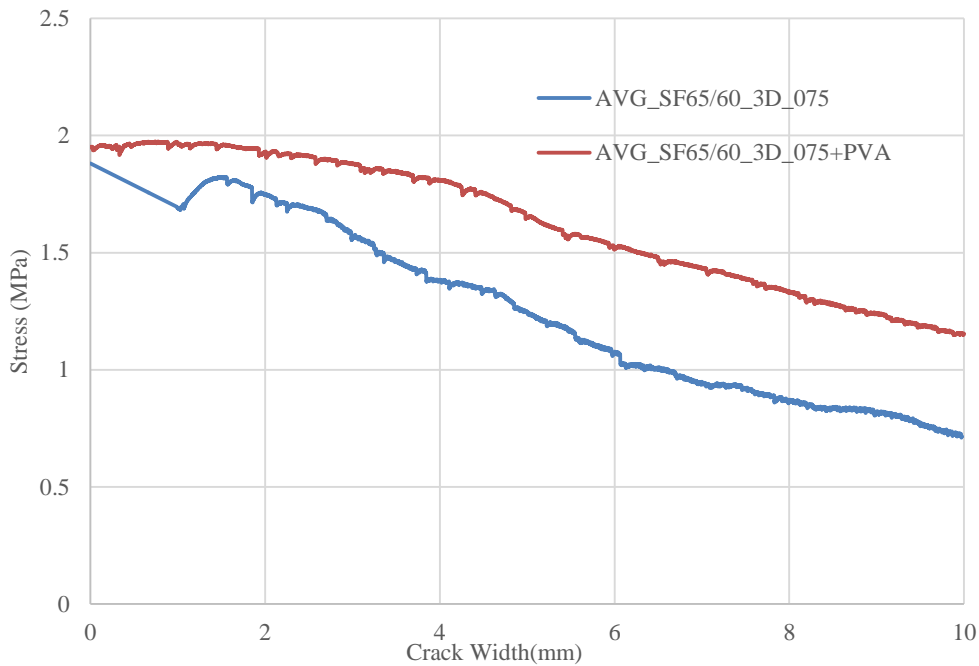


Figure 4.37. Average stress-crack width curves

4.3.3. SF65/60_5D_075 and SF65/60_5D_075+PVA Mixtures

Average stress-crack width behavior of SF65/60_5D_075 and SF65/60_5D_075+PVA is compared in Figure 4.38. PVA addition dropped the average tensile cracking strength by about 7% and consumed energy by about 2%. Both groups have a very similar stress-crack width behavior. However, SF65/60_5D_075+PVA sustained slightly lower levels of tensile stress for crack widths larger than about 6 mm. It has to be noted that only two specimens yielded a dependable test result for SF65/60_5D_075+PVA group. Therefore, a different result could be obtained if more specimens could be tested. On the other hand, it is safe to say that adding PVA did not enhance the tension behavior, although total fiber volume has increased. Inefficiency of PVA's can be attributed to the local balling of PVA's around the double-hook ends of

steel fibers. Another factor could be the already strong anchorage of steel fibers due to their double-hook ends, such that adding PVA does not provide an extra benefit to already strong anchorage.

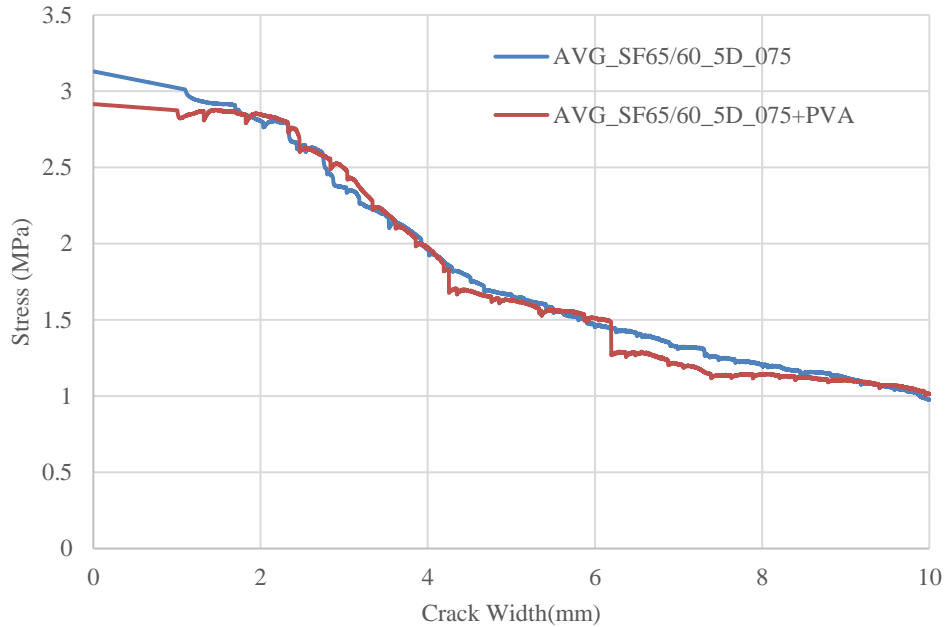


Figure 4.38. Average stress-crack width curves

4.3.4. SF65/60_3D_125 and SF65/60_3D_125+PVA Mixtures

Average stress-crack width behavior of SF65/60_3D_125 and SF65/60_3D_125+PVA is compared in Figure 4.39. Adding PVA to SF65/60_3D_125 dropped the tensile cracking strength by about 19% and energy consumed by about 9%. SF65/60_3D_125+PVA sustained considerably lower level of tensile stresses until about 7 mm crack width. It has to be noted that mix using same type of steel fibers with lower fiber ratio, SF65/60_3D_075, showed an enhanced behavior when PVA's were added. However, when steel fiber ratio was increased as in SF65/60_3D_125, adding PVA's had a considerably detrimental effect. This can be attributed the decreased workability, decreased compaction quality and consequently more heterogeneous structure in the specimen due to clustering and balling of fibers in this high level of fiber ratio.

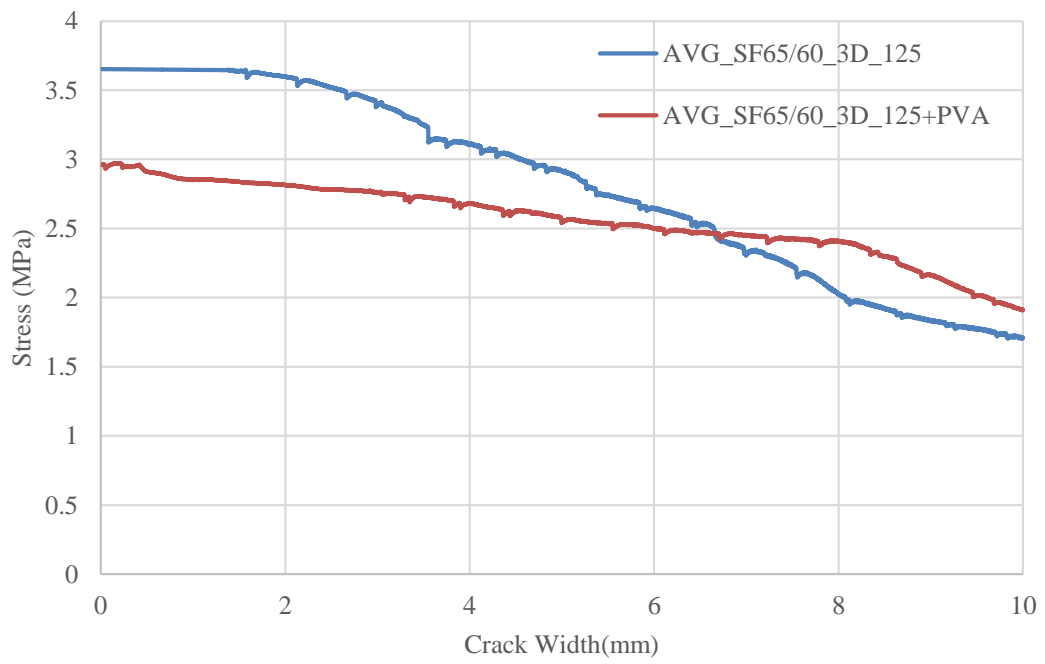


Figure 4.39. Average stress-crack width curves

CHAPTER 5

CONCLUSIONS

In this study, the effects of different fiber types, fiber lengths and fiber ratios on the mechanical behavior of hybrid fiber reinforced concrete under direct tension was investigated. Three different types of steel fibers and PVA fibers in varying ratios were used in the hybrid fiber reinforced concrete. Four different mix designs with steel and PVA fibers, a group with only PVA fibers and a control group without any fibers were cast and tested under direct tension. Stress-crack width responses of steel fiber and steel-PVA hybrid fiber specimens were obtained and compared. Following conclusions were obtained as a result of this study.

1. Synergy between steel and PVA fibers under direct tension was found to be dependent on fiber type and ratio. Addition of PVA fibers did not have a considerable effect with 35 mm single hook and 60 mm double hook steel fibers with 0.75% ratio. PVA addition adversely affected the direct tension response of 60 mm single hook steel fibers with higher 1.25% ratio. A considerable positive synergy was observed only for 60 mm single hook steel fibers with 0.75% ratio.
2. When overall stress levels are concerned, it was seen that long fibers with higher ratio performed better than all others. For specimens without PVA and with the same ratio and same lengths steel fiber, double hook steel fibers performed better compared to single hook steel fibers, possibly due to their better anchorage levels. Shorter steel fibers performed worst although they had the same ratio.
3. With PVA addition, 60 mm double-hook fibers of 0.75% ratio caught stress levels of same length fibers with 1.25% ratio. However, that was not a result of PVA fibers' improving the behavior of double-hook fibers, but because of their detrimental effect on the 1.25% steel fiber ratio mix.
4. PVA addition was most beneficial to 60 mm single hook fibers with 0.75% ratio. But contribution of PVA fibers was not significant enough to reach stress levels of same ratio double-hook or higher ratio single-hook fibers without

PVA. Therefore, when a concrete mix with a certain direct tension performance was sought, it can be said that using longer fibers with higher ratios without PVA is the best option. Although PVA addition contributes the post cracking behavior for lower steel fiber ratios, it also comes with a cost. Trying better performance from steel fibers, such as one with double hook, may be more economical.

5. PVA addition did not change the direct tension behavior of shorter 35 mm single hook steel fibers. Concrete reinforced with these fibers could sustain the lowest levels of tensile stresses regardless of presence of PVA. Therefore, using shorter steel fibers seems to be the least economical option when good direct tension performance was desired.
6. Addition of fiber in the mix did not have a considerable effect on the compressive strength. On the other hand, addition of PVA to the mix with steel fibers decreased the compressive strength in general. Plain concrete control specimen and the specimen with only PVA fibers had very close compressive strengths. Therefore, it can be said that the PVA fibers alone did not affect the compressive strength.
7. As a last remark, it should be noted concrete used in this study had a compressive strength around 30 MPa and a maximum aggregate size of 12 mm, reflecting an ordinary concrete mixture. There is an extensive literature about higher strength fiber reinforced concrete with finer aggregate size that makes a very efficient use of short PVA fibers by providing better anchorage in a stronger matrix. Such concrete materials, commonly called Engineered Cementitious Concrete (ECC), proven to provide a much favorable behavior in terms cracking, durability and ductility (Sahmaran and Li, 2010; Sahmaran and Li, 2009; Banyhussan et al., 2019; Alyousif et al, 2016). Therefore, conclusions obtained from this study are limited to more common ordinary concrete mixes and cannot be generalized to other possible uses of steel and PVA fibers in a hybrid fiber reinforced concrete mix.

REFERENCES

- ACI Committee 544. "State-of-the-Art Report on Fiber Reinforced Concrete." American Concrete Institute, 2002.
- ACI Committee 544. "Design Consideration for Steel Fiber Reinforced Concrete" American Concrete Institute, 1999.
- Alami, Mohammad Musa, Tahir Kemal Erdem, Mert Yücel Yardımcı, and Serdar Aydın. "Development of a proper mix-design for impact loading of deflection hardening hybrid fiber reinforced concrete." In International Conference on Strain-Hardening Cement-Based Composites, pp. 284-291. Springer, Dordrecht, 2018.
- Alberti, M. G., A. Enfedaque, and J. C. Gálvez. "Fibre reinforced concrete with a combination of polyolefin and steel-hooked fibres." *Composite Structures* 171 (2017): 317-325.
- Alyousif, Ahmed, Ozgur Anil, Mustafa Sahmaran, Mohamed Lachemi, Gurkan Yildirim, and Ashraf F. Ashour. "Comparison of shear behaviour of engineered cementitious composite and normal concrete beams with different shear span lengths." *Magazine of Concrete Research* 68, no. 5 (2016): 217-228.
- ASTM, C39. "Standard test method for compressive strength of cylindrical concrete specimens."
- ASTM, C. "Standard test method for splitting tensile strength of cylindrical concrete specimens." C496/C496M-11 (2011).
- Banyhussan, Qais S., Gürkan Yıldırım, Özgür Anıl, Recep T. Erdem, Ashraf Ashour, and Mustafa Şahmaran. "Impact resistance of deflection-hardening fiber reinforced concretes with different mixture parameters." *Structural Concrete* 20, no. 3 (2019): 1036-1050.
- Bentur, Arnon, and Sidney Mindess. *Fibre reinforced cementitious composites*. Crc Press, 2006.
- Caggiano, Antonio, Serena Gambarelli, Enzo Martinelli, Nicola Nisticò, and Marco Pepe. "Experimental characterization of the post-cracking response in hybrid steel/polypropylene fiber-reinforced concrete." *Construction and Building Materials* 125 (2016): 1035-1043.

- Chasioti, Stamatina G., and Frank J. Vecchio. "Effect of Fiber Hybridization on Basic Mechanical Properties of Concrete." *ACI Materials Journal* 114, no. 3 (2017): 375-384.
- Kharal, Zahra. "Tension stiffening and cracking behaviour of GFRP reinforced concrete." PhD diss., 2014.
- Kim, Min Ook, and Amanda Bordelon. Cracking and debonding of a thin fiber reinforced concrete overlay. No. MPC 17-319. Mountain Plains Consortium, 2017.
- Mathew, Bobby A., C. Sudha, P. K. Rajkumar, and P. Ravichandran. "Investigations on tensile properties of high strength steel fibre reinforced concrete." *Indian Journal of Science and Technology* 8, no. 28 (2015): 1-6.
- Naaman, Antoine E., and Hans-Wolf Reinhardt. "Proposed classification of HPFRC composites based on their tensile response." *Materials and structures* 39, no. 5 (2006): 547-555.
- RILEM TC 162-TDF: Test and design methods for steel fibre reinforced concrete: bending test. Final recommendation *Materials and Structures* (2002): 579-582 ISSN 1359-5997.
- Şahmaran, Mustafa, and Victor C. Li. "Engineered cementitious composites: Can composites be accepted as crack-free concrete?." *Transportation Research Record* 2164, no. 1 (2010): 1-8.
- Şahmaran, Mustafa, and Victor C. Li. "Influence of microcracking on water absorption and sorptivity of ECC." *Materials and structures* 42, no. 5 (2009): 593-603.
- Tipka, M., and J. Vašková. "Tensile properties of structural fibre reinforced concrete." In *IOP Conference Series: Materials Science and Engineering*, vol. 246, no. 1, p. 012052. IOP Publishing, 2017.
- Van Vliet, Marcel René Antoine. "Size effect in tensile fracture of concrete and rock." PhD diss., TU Delft, Delft University of Technology, 2000.
- Xu, Lihua, Le Huang, Yin Chi, and Guodong Mei. "Tensile behavior of steel-polypropylene hybrid fiber-reinforced concrete." *ACI Materials Journal* 113, no. 2 (2016): 219-229.
- Yurtseven, Alp Eren. "Determination of mechanical properties of hybrid fiber reinforced concrete." MS. C. Thesis, Graduate School of Natural and Applied Sciences of Middle East Technical University (2004).